Published in final edited form as:

Nature. 2017 May 11; 545(7653): 234–237. doi:10.1038/nature22306.

Surrogate Wnt agonists that phenocopy canonical Wnt/β-catenin signaling

Claudia Y. Janda[1,8], **Luke T. Dang**[2,8], **Changjiang You**[3], **Junlei Chang**[4], **Wim de Lau**[5], **Zhendong A. Zhong**[6], **Kelley S. Yan**[4], **Owen Marecic**[7], **Dirk Siepe**[1], **Xingnan Li**[4], **James D. Moody**[2], **Bart O. Williams**[6], **Hans Clevers**[5], **Jacob Piehler**[3], **David Baker**[2], **Calvin J. Kuo**[4], and **K. Christopher Garcia**[1,*]

[1]Department of Molecular and Cellular Physiology, Howard Hughes Medical Institute, and Department of Structural Biology, Stanford University School of Medicine, Stanford, CA 94305, USA [2]Department of Biochemistry, Howard Hughes Medical Institute, and the Institute for Protein Design, University of Washington, Seattle, WA 98195, USA [3]Division of Biophysics, Department of Biology, University of Osnabrück, 49076 Osnabrück, Germany [4]Department of Medicine, Division of Hematology, Stanford University School of Medicine, Stanford, CA, 94305, USA [5]Hubrecht Institute, Royal Netherlands Academy of Arts and Sciences, and University Medical Center Utrecht, Uppsalalaan 8, 3584 CT, Utrecht, The Netherlands [6]Program for Skeletal Disease and Tumor Microenvironment and Center for Cancer and Cell Biology, Van Andel Research Institute, 333 Bostwick NE, Grand Rapids, MI, 49503, USA [7]Hagey Laboratory for Pediatric Regenerative Medicine and Department of Surgery, Institute for Stem Cell Biology and Regenerative Medicine, Stanford University School of Medicine, Stanford, CA, 94305, USA

Abstract

Wnts modulate cell proliferation, differentiation and stem cell self-renewal, by inducing β-catenin dependent signaling through Frizzled (Fzd) and Lrp5/6 to regulate cell fate decisions, and the growth and repair of a multitude of tissues[1]. The 19 mammalian Wnts interact promiscuously with the 10 Fzds, which has complicated the attribution of specific Fzd/Wnt subtype interactions to distinct biological functions. Furthermore, Wnts are post-translationally modified by

*Corresponding author: K. Christopher Garcia (kcgarcia@standord.edu).
[8]These authors contribute equally to this work

Data availability statement

Structure factors and coordinates have been deposited to the Protein Data Bank under accession numbers 5UN5 and 5UN6. All other data are available from the corresponding author upon reasonable request.

Author contributions

C.Y.J. designed experiments, performed biophysical measurements, determined crystal structures, performed *in vitro* functional assays and prepared the manuscript. D.S. analyzed data. D.B., L.T.D. and J.D.M. designed B12, and performed affinity maturation. J.P. and C.Y. performed TIRF microscopy, analyzed data and contributed to manuscript preparation. Z.A.Z. and B.O.W. performed osteogenesis assays, and analyzed data. W.d.L. and H.C. performed organoid culture assays, analyzed data and contributed to manuscript preparation. J.C., K.S.Y. and X.L. carried out in vivo experiments in mice and analyzed data. O.M. performed parabiosis surgery. C.J.K. designed and supervised in vivo experiments, analyzed data and contributed to manuscript preparation. K.C.G. conceived of the project, analyzed data, supervised execution of the project, and prepared the manuscript.

Competing Financial Interests:

KCG, CK, and CJ are founders of Surrozen Therapeutics, which is attempting to commercialize the Wnt surrogates for clinical use.

palmitoylation, which is essential for Wnt secretion and functions as a critical site of interaction with Fzd [2–4]. As a result of their acylation, Wnts are very hydrophobic proteins requiring detergents for purification, which presents major obstacles for the preparation and application of recombinant Wnts. This has hindered the delineation of the molecular mechanisms of Wnt signaling activation, understanding of the functional significance of Fzd subtypes, and the use of Wnts as therapeutics. Here we developed surrogate Wnt agonists, water-soluble Fzd-Lrp5/6 heterodimerizers, consisting of Fzd5/8-specific and broadly Fzd-reactive binding domains, that elicit a characteristic β-catenin signaling response in a Fzd-selective fashion, enhance osteogenic lineage commitment of primary mesenchymal stem cells (MSCs), and support the growth of a broad range of primary human organoid cultures comparably to Wnt3a. Furthermore, we demonstrate that the surrogates can be systemically expressed and exhibit Wnt activity *in vivo,* regulating metabolic liver zonation and promoting hepatocyte proliferation, resulting in hepatomegaly. These surrogates demonstrate that canonical Wnt signaling can be activated simply through bi-specific ligands that induce receptor heterodimerization. Furthermore, these easily produced non-lipidated Wnt surrogate agonists offer a new avenue to facilitate functional studies of Wnt signaling and the exploration of Wnt agonists for translational applications in regenerative medicine.

The direct engagement of the Wnt lipid by the Fzd-CRD, and the extremely unusual fold of Wnt proteins (Fig. 1a)[4] presented a sub-optimal scaffold to re-engineer Wnt as a water-soluble protein, so we developed a strategy to engineer surrogate proteins that are structurally unrelated to Wnts. While forced heterodimerization of genetically modified Fzd and Lrp5/6 can enhance signaling [5–8], it remains unclear whether intrinsic structural properties of Wnt, or natural ligands like Norrin, are required for normal canonical signaling, and whether dimerization alone by an enginneered ligand would be sufficient for signaling activation. We engineered water-soluble Wnt agonists by linking antagonistic Fzd and Lrp5/6-binding modules into a single polypeptide chain, thus forcing receptor heterodimerization while blocking endogenous Wnt binding (Fig. 1a). We used Fzd subtype-specific and cross-reactive binding modules for restricted and broad cell-type specificity, respectively. For the Fzd subtype-specific binder, through an integration of *de novo* design and protein engineering using yeast surface display, we created B12, a 4-helix bundle domain protein derived from *Bacillus Halodurans*, which binds specifically to Fzd5 and 8, two closely related Fzds, with relative affinities of 9 and 18 nM (Fig. 1a,b and Extended Data Fig. 1, 2a–c). The crystal structure revealed that B12 binds Fzd8-CRD at the rim of the lipid-binding groove engaging the Fzd5/8 specific Trp73 as hotspot residue. Leu57 and Leu62 in the loop following helix 2 bind to the groove, resulting in partial overlap with the Wnt lipid-binding site, and weak Wnt antagonism (Fig. 1c and Extended Data Fig. 2d). For the Fzd cross-reactive analog, we used the single-chain variable fragment (scFv) of the Wnt antagonizing antibody Vantictumab, which binds Fzd1, 2, 5, 7 and 8 with high affinity (0.7 – 1.4 nM) (Fig. 1b and Extended Data Fig. 2e–h)[9]. To create Fzd-Lrp5/6 heterodimerizers, we linked the Fzd binding modules (B12, scFv) to the C-terminal domain of human Wnt antagonist DKK1. This C-terminal domain, which is sufficient for Wnt inhibition and binds Lrp5/6 with moderate affinity (20–70 nM)[10,11], was linked to B12 and scFv, through a flexible Gly-Ser polypeptide linker (these fusions are referred to as B12-DKK1c and scFv-DKK1c throughout) of 0– 15 amino acids, and 5 amino acids, respectively (Fig. 1a).

To interrogate whether the surrogates heterodimerize and cluster Fzd and Lrp5/6 on live cell surfaces comparably to Wnts[11,12], we probed the assembly and diffusion dynamics of Fzd8 and Lrp6 upon the addition of Wnts and surrogates by dual-color single-molecule fluorescence imaging. Fzd8 and Lrp6 fused to an N-terminal SNAP-tag and Halo-tag, respectively, were transiently expressed in HeLa cells and labeled with Dy649 and TMR (Fig. 1d)[13]. IWP-2, an inhibitor of endogenous Wnt secretion reduced the basal low levels of receptor co-localization (Extended Data Fig. 3a and Supplementary Video 1). Upon addition of scFv-DKK1c, B12-DKK1c, XWnt8 and Wnt3a, Fzd8-Lrp6 complexes with reduce mobility were detected by co-locomotion and single complex trajectories analysis (Fig. 1d–e and Extended Data Fig. 3b–c, 4, Supplementary Video 2–5). In addition, rates of Fzd8/Lrp6 dimerization and β-catenin accumulation induced by Wnts and surrogates correlate well (Extended Data Fig. 3d–j). Moreover, complexes with increased intensities were observed, confirming comparable Fzd8 and Lrp6 oligomerization by Wnts and Wnt surrogates (Extended Data Fig. 5).

To determine whether the surrogate proteins elicited Fzd-specific activation of canonical Wnt signaling, we performed a series of reporter assays. scFv-DKK1c, but not B12-DKK1c, XWnt8 or negative controls, activated Wnt signaling in L cells (expressing Fzd7), which can be sensitized to B12-DKK1c and XWnt8 by specifically over-expressing Fzd5 or 8 (Fig. 2a–c and Extended Data Fig. 6a). While Wnt signaling in A375 and SH-SY5Y cells (expressing Fzd2), was robustly induced only by scFv-DKK1, both surrogates induced reporter expression in A549 cells (expressing Fzd2, 4, 6, and 8) (Extended Data Fig. 6b–d). In agreement with their specificities, B12-DKK1c and scFv-DKK1c were antagonized by neutralizing (Fzd8-CRD-Fc vs Fzd1/8-CRD-Fc) and blocking (isolated DKK1, B12 vs DKK1) domains (Extended Data Fig. 6e–f). Furthermore, scFv-DKK1c triggered Lrp6 phosphorylation, and accumulation of β-catenin in A375 cells, comparable to Wnt3a conditioned media (CM), characteristic of canonical Wnt pathway activation (Extended Data Fig. 2g). In addition, scFv-DKK1c and B12-DKK1c enhanced the transcription of the universal Wnt target gene *Axin2* in SH-SY5Y, and A549 cells, respectively, similar to control Wnts (Extended Data Fig. 6h–i). Interestingly, B12-DKK1c with different linkers display differential activity as reflected in signaling amplitudes (Extended Data Fig. 6i–j) demonstrating that the surrogate's signal strength can be 'tuned' by variations in proximity of the binding modules. In HEK293 cells, RSPO2 strongly potentiates the activity of scFv-DKK1c, comparable to Wnt3a-CM (Fig. 2d)[14], adding further validation to the surrogates signaling in a "Wnt-like" mechanism. Furthermore, a single-chain fusion protein comprised of RSPO2 linked to the C-terminal end of scFv-DKK1c, replicates the enhanced activity of the combination (Fig. 2d).

Given that Wnt signaling plays a pivotal role in bone formation[15] we evaluated the activity of the Wnt surrogates on MSCs. scFv-DKK1c and scFv-DKK1c-RSPO2 enhanced the dose-dependent up-regulation of the early osteogenesis marker *alkaline phosphatase* (*ALP*) in mouse C3H10T1/2 multipotent MSCs (mRNA and enzymatic activity) (Extended Data Fig. 7a,b). In agreement with recent reports[16], Wnt3a and Wnt surrogates synergize with BMP2 to enhance ALP up-regulation, while suppressing BMP2 induced chrondrogenisis marker *collagen 2A1* (*Col2A1*) (Fig. 2e and Extended Data Fig. 7c–d). A synergistic ALP up-regulation was also observed in primary human MSCs (mRNA and enzymatic activity) and

mouse MSC (enzymatic activity) (Fig. 2f and Extended Data Fig. 7e–h), suggesting the possibility that the Wnt surrogates could be therapeutic candidates to enhance bone regeneration.

In the presence of the required niche factors, including Wnt3a and Rspo, adult stem cells can develop into 3D organoids that resemble their corresponding organs, recapitulating their regenerative capacity *ex vivo*[17–20]. To test whether scFv-DKK1c could substitute for Wnt3a, we grew organoids from single cell suspensions of normal human tissues in the presence or absence of recombinant scFv-DKK1c, scFv-DKK1c-RSPO2, Wnt3a CM, RSPO3 CM and IWP-2. Pancreas, stomach, colon and liver produce endogenous Wnts, and organoids grow in the presence of RSPO3, and absence of exogenous Wnt, which is suppressed by IWP-2 (Fig. 3 and Extended Data Fig. 8a–e). In the presence of IWP-2, scFv-DKK1c and scFv-DKK1c-RSPO2 were superior or comparable to Wnt3a CM in promoting the continuous growth of organoids derived from the pancreas, colon and stomach (corpus), yet, they were less active in supporting the growth of liver organoids (Fig. 3 and Extended Data Fig. 8a–e). The differential activity might be attributed to differential Fzd specificity, and unknown factors in the CM. Intestinal organoids represent a model for personalized cystic fibrosis (CF) drug screening[21]. While intestinal organoids from healthy donors swell upon the opening of cystic fibrosis transmembrane conductance regulator (CFTR) channels by cAMP, cystic fibrosis organoids will only swell when pretreated with CFTR activating/stabilizing drugs. Wnt surrogates supported the growth of strongly budded organoids, in a comparable manner to Wnt3a (Extended Data Fig. 8f), yet offer the opportunity to culture organoids in defined media, circumventing the interference of unknown components with the assay.

To assess the activities of Wnt surrogates *in vivo*, we used a recombinant adenoviral expression system to systemically deliver scFv-DKK1c and scFv-DKK1c-RSPO2 in mice. When injected intravenously (i.v.), adenovirus infects hepatocytes, resulting in durable expression of the transgenes[22]. In the liver Wnts are expressed around the central vein[23], and activate a Wnt-driven pericentral gene expression program, such as *glutamine synthetase* (*GS*) in hepatocytes immediately adjacent to the source, resulting in metabolic zonation[24]. We infected wild type C67Bl/6J mice with Ad scFv-DKK1c, Ad scFv-DKK1c-RSPO2, Ad Wnt3A, RSPO2-Fc or murine IgG2a Fc fragment (Ad Fc) as negative control (n=4mice/group). Infection of the liver was confirmed by qRT-PCR, and circulating scFv-DKK1c and scFv-DKK1c-RSPO2 proteins (Extended Data Fig. 9a–f), but not Wnt3A (data not shown) was detected in the peripheral blood. After 7 days, Ad scFv-DKK1c, Ad RSPO2-Fc and Ad Wnt3A modestly expanded the GS-expressing region, while repressing the periportal marker *Cyp2f2* (inhibited by Wnt pathway activation) and inducing *Axin2* mRNA compared to control mice (Fig. 4a–b and Extended Data Fig. 9g–i). Notably, Ad scFv-DKK1c + Ad RSPO2-Fc, Ad scFv-DKK1c-RSPO2 and to a lesser extend Ad Wnt3A + Ad RSPO2-Fc elicited a synergistic induction of GS (in ~90% of the liver lobule) and Axin2 expression and suppression of Cyp2f2 mRNA (Fig. 4a–b and Extended Data Fig. 9g–i).

To examine the effect of scFv-DKK1c or scFv-DKK1c-RSPO2 on hepatocyte proliferation we infected adult C57Bl/6J mice (donor mice) with Ad scFv-DKK1c, Ad scFv-DKK1c-RSPO2 or Ad Fc followed by parabiosis where the circulatory systems of two mice are conjoined (Extended Data Fig. 10a). While *scFv-DKK1c* and *scFv-DKK1c-RSPO2* mRNA

was detected in the livers of donor mice, serum scFv-DKK1c and scFv-DKK1c-RSPO2 proteins, enhanced liver *GS* and *Axin2* expression, and reduced liver *Cyp2f2* expression were present in donor and recipient mice (Extended Data Fig. 10b–i) confirming that adenoviral infection was confined to the donor. The livers in recipient scFv-DKK1c and scFv-DKK1c-RSPO2 treated mice exhibited mild hepatomegaly and significant increased proliferation of HNF4α-positive hepatocytes in all hepatocyte zones most pronounced in the periportal region, similar to recent observations with R-spondin[25] (Fig. 4c–d and Extended Data Fig. 10j). Therefore, these surrogates activate Wnt signaling *in vivo*, altering Wnt-driven hepatic metabolic zonation and proliferation. Given the tight feedback regulation of the Wnt pathway, indirect effects cannot be entirely ruled out. Furthermore, an accompanying study demonstrates that the Wnt surrogates induce proliferation of intestinal crypt cells, confirming their activity on tissues distant from the site of protein production (see companion paper by Yan et al.).

The development of surrogate Wnt agonists offers both conceptual insight into Wnt signaling and a practical advance for experimental and therapeutic applications. The ability of the bi-specific heterodimerizer scFv-DKK1c, which concurrently blocks endogenous Wnt binding, to faithfully mimic Wnt activity demonstrates that Fzds and Lrp5/6 follow the paradigm of signaling activation through receptor dimerization, as seen for growth factor and cytokine receptors[26,27]. The relative orientations and proximities of the receptors induced by Wnt ligands, and the surrogates, are likely the principle parameters determining the efficiency of signal initiation. However, we cannot rule out that natural Wnts, and also the cysteine-knot growth factor Norrin which activates canonical Wnt signaling through Fzd4 and Lrp5/6 oligomerization[28–30], may possess intrinsic structural features that initiate additional or alternative signaling outcomes, such as perhaps by inducing ligand-specific conformational changes in Fzd. Future experiments more deeply investigating the signaling and functional properties of Wnts versus the surrogates will clarify such questions. The ease of Wnt surrogate production, and their ability to target specific Fzd sub-types may allow for a better control of Wnt/Fzd pleiotropy, facilitating the introduction of Wnt agonism into the clinic for regenerative medicine applications.

Methods

Cell lines

HEK293 cells stably transfected with the STF plasmid encoding the firefly luciferase reporter under the control of a minimal promoter and a concatemer of seven LEF/TCF binding sites[31], were obtained from Prof. Jeremy Nathans. Mouse L cells stably transfected with the STF plasmid, and a constitutively expressed renilla luciferase (control reporter), was obtained from Prof Calvin Kuo. L cells transfected with a mouse Wnt3a expression vector to produce CM was obtained from ATCC. A375, SH-SY5Y and A549 cells were stably transfected with the BAR plasmid encoding the firefly luciferase reporter under the control of a minimal prompter and a concatemer of 12 TCF/LEF binding sites, and a constitutively expressed renilla luciferase (control reporter) using a lentiviral-based approached 32. All reporter cell lines were cultured in complete DMEM medium (Gibco) supplemented with 10 % FBS, 1% Penicillin, Streptomycin, and L-Glutamine (Gibco), at

37°C and 5 % CO2 and cultured in the presence of antibiotics for selection of the transfected reporter plasmid. C3H10T1/2 cells were obtained from ATCC. Human primary MSCs were obtained from Cell Applications, Inc. Mouse primary MSCs were obtained from Invitrogen. Cell lines have not been tested for mycoplasma contamination.

Protein constructs, expression and purification

The coding sequence of B12 containing a C-terminal 6xHis-tag was cloned into the pET28 vector (Novagen) for bacterial cytoplasmic protein expression. Protein expression was performed in transformed BL21 cells, expression was induced with 0.7 mM IPTG at an OD600 for 3–4 hours. Cells were pelleted, lysed by sonication in lysis buffer (20 mM HEPES pH 7.2, 300 mM NaCl, 20 mM Imidazole), and soluble fraction was applied to Ni-NTA agarose (QIAGEN). After washing the resin with lysis buffer containing 500 mM NaCl, B12 was eluted with 300 mM Imidazole, and subsequently purified on a Superdex 75 size-exclusion column (GE Healthcare) equilibrated in 1xHBS (10 mM Hepes pH 7.2, 150 nM NaCl).

XWnt8 was purified from a stably transfected Drosophila S2 cell line co-expressing XWnt8 and mouse Fzd8-CRD-Fc described previously [4]. Cells were cultured in complete Schneider's medium (Thermo Fisher Scientific), containing 10 % FBS and supplemented with 1% L-Glutamine, Penicillin and Streptomycin (Gibco), and expanded in Insect-Xpress medium (Lonza). The XWnt8/Fzd8-CRD-Fc complex was captured from the CM on Protein A agarose beads (Sigma). After washing with 10 column volumes 1xHBS, XWnt8 was eluted with 1xHBS containing 0.1 % n-dodecyl β-D-maltoside (DDM) and 500 mM NaCl, while the Fzd8-CRD-Fc remained bound to the beads.

All other proteins were expressed in High Five (*Trichoplusia ni*) cells (Invitrogen) using the baculovirus expression system. To produce the B12-based surrogate, the coding sequences of B12, a flexible linker peptide comprising of 0, 1, 2 or 3 GSGSG-linker repeats, followed by the C-terminal domain of human DKK1 (residues 177 – 266), and a C-terminal 6xHis-tag, were cloned into the pAcGP67A vector (BD Biosciences, San Diego, CA). To clone the scFv-based surrogate ligand, the sequence of the Vantictumab was retrieved from the published patent, reformatted into a scFv, and cloned at the N-terminus of the surrogate variant containing the GSGSG linker peptide. To produce recombinant Fzd-CRD for crystallization, surface plasmon resonance measurements, SEC-MALS experiments and functional assays, the CRDs of human Fzd1 (residues 113 – 182), human Fzd4 (residues 42–161), human Fzd5 (residues 30 – 150), human Fzd7 (residues 36 – 163), human Fzd8 (residues 32–151) and human Fzd10 (residues 30–150), containing a C-terminal 3C protease cleavage site (LEVLFQ/GP), a biotin acceptor peptide (BAP)-tag (GLNDIFEAQKIEWHE) and a 6xHis-tag were cloned into the same vector. The human Fzd8-CRD for crystallization contained only a C-terminal 6xHis-tag, in addition to a N49E mutation to mutate the N-linked glycosylation site. Fzd1/8-CRD for inhibition assay contained a C-terminal 3C protease cleavage site, Fc-tag (constant region of human IgG), and a 6xHis-tag. Human DKK1 (residues 32 – 266) with a C-terminal BAP-tag and 6xHis-tag, and the two furin-like repeats of human RSPO2 (residues 36–143) with a N-terminal Fc-tag and a C-terminal 6xHis-tag, were cloned also into the pAcGP67A vector. All proteins were secreted from

High Five insect cells grown in Insect-Xpress medium, and purified using Ni-NTA affinity purification, and size exclusion chromatography equilibrated in 1xHBS (10 mM HEPES pH 7.3, 150 nM NaCl). Enzymatic biotinylation was performed in 50 mM bicine pH 8.3, 10 mM ATP, 10 mM $Mg(OAc)_2$, 0.5 mM d-biotin with recombinant GST-BirA ligase overnight at 4°C, and proteins were subsequently re-purified on a Superdex 75 size-exclusion column to remove excess biotin.

Computational design of Fzd8-specific binding domain

We attempted to mimic the native Wnt-Frizzled lipid-protein interaction with a *de novo* designed protein-protein binding interface. A thirteen residue alanine helix was docked against the lipid-binding cleft using Foldit [33]. This structural element was grafted onto a diverse set of native helical proteins using the Rosetta Epigraft [34] application in order to discover scaffolds with compatible, shape-complementary backbones. Prototype designs were selected by interface size and optimized using RosettaScripts [35] to perform sidechain redesign. Fifty selected designs were further manually designed to ensure charge complementarity and non-essential mutations were reverted to the wild-type amino acid identity in order to maximize stability. DNA was obtained from Gen9 and screened for binding via yeast surface display as previously described with 1μM biotinylated Fzd8-CRD pre-incubated with SAPE (Life Technologies) [36]. A design based on the 2QUP scaffold, a uncharacterized four helix bundle protein from *Bacillus Halodurans*, demonstrated binding activity under these conditions, while knockout mutants A173R and A174D made using the Kunkel method [37] abrogated binding, verifying that the functional interface utilized the predicted residues. Wild-type scaffold 2QUP did not bind, confirming that activity was specifically due to design.

Affinity maturation of B12

In order to improve the affinity of the original design, a full-coverage site saturation mutagenesis (SSM) library was constructed for design based on the 2QUP scaffold via the Kunkel mutagenesis method [37] utilizing forward and reverse primers containing a ‘NNK’ degenerate codon and 21 bp flanking regions (IDT). A yeast library was transformed as previously described [38] and sorted for 3 rounds, collecting the top 1% of binders using the BD Influx cell sorter. Naïve and selected libraries were prepared and sequenced, and the data processed as previously described [38] using a Miseq (Illumina) according to manufacturer protocols. The most enriched eleven mutations comparing the selected and unselected pools of binders were combined in a degenerate library containing all enriched and WT amino acid identities at each of these positions. This combination library was assembled from the oligos (IDT) listed below for a final theoretical diversity of ~800k distinct variants. This library was amplified, transformed, and selected to convergence over five rounds, yielding the optimized variant B12.

>Ultramer1_fwd_164bp

GCTAGTGGTGGAGGAGGCTCTGGTGGAGGCGGTAGCGGAGGCGGAGGGTC
GGCTAGCCATATGGGCGTGAGCTTTAGCGAAGTGATGGGCAAACAGAAAG
ATGAACAGGCGCGTGAACAGCTGAAAGAAGGCATGAWAAAAATTGAAGA
ACAGGGCAAAAAGCT

>Ultramer2_rev_133bp

AGCCACGACGTTCTTCCAGATTCKKTCCCAGAAAACCCGCCKSCRMCGCA
AAARBCGCCACCGCTGCGRCATATTTCTGCAGCTCTTCCTGGGTACGGGTT
TCGCTCAGCTTTTTGCCCTGTTCTTCAATTTT

>Ultramer3_fwd_147bp

AATCTGGAAGAACGTCGTGGCTTTAATCGTCGGGGCAAAGAAGAAATTGG
CAAAATTAGCGGAGAAGTGTACMWAAAACTGTTAGACCTGAAAAAAGCGG
TGCGTGCGAAAGAAAAAAAGGGACTGGATATTCTGAATATGGTGGGC

>Ultramer4__rev_128bp

GTTGTTATCAGATCTCTATTACAAGTCCTCTTCAGAAATAAGCTTTTGTTCGG
ATCCGCCCCCCTCGAGCGCAKRAMYACKCTCCAGGRKGCCCTTAATCTCGC
CCACCATATTCAGAATATCCAGTC

Complex crystallization and structure determination

The B12-Fzd8CRD-N49Q complex was formed by mixing purified B12 and Fzd8CRD-N49E in stoichiometric quantities. The complex was then treated with 1:100 (w/w) carboxypeptidase A (Sigma) overnight at 4°C, and purified on a Superdex 75 (GE Healthcare Life Sciences) size-exclusion column equilibrated in 1xHBS. Purified complex was concentrated to ~ 15mg/ml for crystallization trials. Crystals were grown by hanging-drop vapor diffusion at 295 K, by mixing equal volumes of the complex and reservoir solution containing 42–49% PEG 400, 0.1 M Tris pH 7.8–8.2, 0.2 M NaCl, or 20% PEG 3000, 0.1 M Sodium citrate pH 5.5 While the PEG 400 condition is already a cryo-protectant, the crystals grown in the PEG 3000 condition were cryoprotected in reservoir solution supplemented with 20 % glycerol before flash freezing in liquid nitrogen. Crystals grew in space groups $P2_1$ (PEG 400 condition) and P2 (PEG 3000 condition), respectively, with 2 and 4 complexes in the asymmetric units. Cell dimensions are listed in Extended Data Table 1. Data were collected at beamline 8.2.2 at the Advanced Light Source (ALS), Lawrence Berkeley National Laboratory. All data were indexed, integrated, and scaled with the XDS package [39]. The crystal structures in both space groups were solved by molecular replacement with the program PHASER [40] using the structure of the Fzd8CRD (PDB ID 1IJY) and the designed model of a minimal core of B12 as search models. Missing residues were manually build in COOT [41] after initial rounds of refinement. Several residues at the N-terminus (residues 1 to 16/17/20/21), at the C-terminus (residues after 117) and several residues within loop regions were unstructured and could not been modeled. Furthermore, we observed that in both crystal forms, B12 underwent domain swapping, and one B12 molecule lent helix 3 and 2 to another B12, resulting in a closely packed B12 homodimer. The density of the loops connecting helix 1 and 2, and 3 and 4 were clearly visible, and folded into helical turns. Yet, SEC-MALS experiments confirmed that B12 existed as a monomer in solution, and complexed Fzd8-CRD with a 1:1 stoichiometry. PHENIX Refine [42] was used to perform group coordinate refinement (rigid body refinement), followed by individual coordinate refinement using gradient-driven minimization applying stereo-chemical restraints, NCS restraints, and optimization of X-ray/stereochemistry weight, and individual B-factor refinement. Initial rounds of refinement were aided by restraints from the

high-resolution mouse Fzd8-CRD structure as a reference model. Real space refinement was performed in COOT into a likelihood-weighted SigmaA-weighted 2mFo-DFc map calculated in PHENIX. The final model in the P2 space group was refined to 3.20 Å with R_{work} and R_{free} values of 0.2002 and 0.2476, respectively (Supplementary Table 1). The quality of the structure was validated with MolProbity [43]. 99.5 % of residues are in the favored region of the Ramachandran plot, and no residue in the disallowed region. The structure within the $P2_1$ space group was refined to 2.99 Å with R_{work} and R_{free} values of 0.2253 and 0.2499 respectively, with 99.2 % of residues in the favored region of the Ramachandran plot, and no residues in the disallowed region. See Supplementary Table 1 for data and refinement statistics. Structure figures were prepared with the program PYMOL.

Affinity measurements of B12 and scFv-DKK1c interaction with Fzd-CRDs

Binding measurements were performed by surface plasmon resonance on a BIAcore T100 (GE Healthcare) and all proteins were purified on SEC prior to experiments. Biotinylated Fzd1-CRD, Fzd5-CRD, Fzd7-CRD and Fzd8-CRD were coupled at a low density to streptavidin on a SA sensor chip (GE Healthcare). An unrelated biotinylated protein was captured at equivalent coupling density to the control flow cells. Increasing concentrations of B12 and scFv-DKK1c were flown over the chip in 1xHBS-P (GE Healthcare) containing 10 % glycerol and 0.05 % BSA at 40 µl/ml. The chip surface was regenerated after each injection with 2 M $MgCl_2$ in HBS-P or 50 % EG in HBS-P (scFv-DKK1c measurements), or 4 M $MgCl_2$ in HBS-P (B12 measurements) for 60 seconds. Curves were reference-subtracted and all data were analyzed using the Biacore T100 evaluation software version 2.0 with a 1:1 Langmuir binding model to determine the K_D values.

Analysis of yeast displayed B12 binding to human Fzd-CRDs

To characterize Fzd-specificity of B12, the yeast display vector encoding B12 was transformed into EBY100 yeast. To induce the display of B12 on the yeast surface, cells were growing in SGCAA medium [44,45] for 2 days at 20°C. 1×10^6 yeast per condition were washed with PBE (1xPBS, 0.5 % BSA, 2 mM EDTA), and stained separately with 0.06 – 1000 nM biotinylated Fzd1/4/5/7/8/10-CRD for 2 hrs at 4°C. After washing twice with ice-cold PBE, bound Fzd-CRDs were labeled with 10 nM strapdavidin-Alexa647 for 20 min. Cells were fixed with 4% paraformaldehyde, and bound Fzd-CRD was analyzing on an Accuri C6 flow cytometer.

Plasmids, cell culture and cell labeling for single molecule fluorescence microscopy

Fzd8 fused to an N-terminal HaloTag® [46] and Lrp6 fused to an N-terminal SNAPTag® [47] were cloned into the pSEMS-26m vector (Covalys Biosciences) by cassette cloning [48,49]. The template pSEMS-26m vectors had been coded with DNA sequences of the $SNAP_f$-tag® or the HaloTag®, respectively, together with an Igκ leader sequence (from the pDisplay vector, Invitrogen) as described previously [49]. The genes of full length mouse Fzd8 and human Lrp6 without the N-terminal signal sequences were inserted into pSEMS-26m via *XhoI* and *AscI*, or *AscI* and *NotI* restriction sites, respectively. A plasmid encoding a model transmembrane protein, maltose binding protein fused to a transmembrane domain, fused to an N-terminal HaloTag was prepared as described recently [50]. HeLa cells were cultivated at

37°C, 5% CO_2 in MEM Earle's (Biochrom AG, FG0325) supplemented with 10% fetal calf serum and 1% nonessential amino acids. Cells were plated in 60 mm cell culture dishes to a density of 50% confluence and transfected via calcium phosphate precipitation [48]. 8–10 h post transfection, cells were washed twice with PBS-buffer and the medium was exchanged, supplied with 2 μM porcupine inhibitor IWP-2 for inhibiting maturation of endogenous Wnt in HeLa cells [51]. 24 h post transfection, cells were plated on glass coverslips pre-coated with PLL-PEG-RGD [52] for reducing nonspecific binding of dyes during fluorescence labeling. After culturing for 12 h, coverslips were mounted into microscopy chambers for live cell imaging. SNAPTag and HaloTag were labeled by incubating cells with 50 nM benzylguanine-Dy649 (BG-649 or SNAP-Surface® 649, New England Biolabs) and 80 nM of HaloTag® tetramethylrhodamine ligand (HTL-TMR, Promega) for 20 min at 37°C. Under these conditions, effective degrees of labeling estimated from single molecule assays with a HaloTag-SNAP-tag fusion protein were ~40% for the Dy649/SNAP-tag and ~25 % for the HaloTag [50]. After washing 3 times with PBS buffer, the chamber was refilled with MEM containing 2 μM IWP-2 for single molecule fluorescence imaging.

Single molecule fluorescence microscopy

Single molecule fluorescence imaging was carried out by using an inverted microscope (Olympus IX71) equipped with a triple-line total internal reflection (TIR) illumination condenser (Olympus) and a back-illuminated EMCCD camera (iXon DU897D, 512×512 pixel from Andor Technology). A 561 nm diode solid state laser (CL-561-200, CrystaLaser) and a 642 nm laser diode (Luxx 642-140, Omicron) were coupled into the microscope for excitation. Laser lights were reflected by a quad-line dichroic beam splitter (Di R405/488/561/647, Semrock) and passed through a TIRF objective (UAPO 150×/1.45, Olympus). For simultaneous dual-color detection, a DualView microimager (Optical Insight) equipped with a 640 DCXR dichroic beamsplitter (Chroma) in combination with bandpass filters FF01-585/40 and FF01 670/30 (Semrock), respectively, was mounted in front of the camera. The overlay of the two channels was calibrated by imaging fluorescent microbeads (TetraSpeck™ microspheres 0.1 μm, T7279, Invitrogen), which were used for calculating a transformation matrix. After channel alignment, the deviation between the channels was below 10 nm.

For single molecule imaging, typical excitation powers of 1 mW at 561 nm and 0.7 mW at 642 nm measured at the objective were used. Time series of 150–300 frames were recorded at 30 Hz (4.8–9.6 s). An oxygen scavenging system containing 0.5 $mg \cdot ml^{-1}$ glucose oxidase, 40 $mg \cdot ml^{-1}$ catalase, and 5 % w/v glucose, together with 1 μM ascorbic acid and 1 μM methyl viologene, was added to minimize photobleaching [53]. Receptor dimerization was initiated by incubating with 100 nM of Wnts or surrogates. Images were acquired after 5 min incubation in the presence of the ligands. All live cell imaging experiments were carried out at room temperature.

Receptor heterodimerization analysis

A 2D Gaussian mask was used for localizing single emitters [54,55]. For colocalization analysis to determine the heterodimerization fraction, particle coordinates from two channels were aligned by a projective transformation (*cp2tform* of type 'projective', MATLAB

2012a) according to the transformation matrix obtained from microbead calibration measurement. Particles colocalized within a distance of 150 nm were selected. Only co-localized particles, which could be tracked for at least 10 consecutive frames (i.e. molecules co-locomoting for at least 0.32 s) were accepted as receptor heterodimers or –oligomers, which has been previously found to be a robust criterion for protein dimerization [50]. The fraction of heterodimerization/-oligomerization was determined as the number of co-locomotion trajectories with respect to the number of the receptor trajectories. Since the receptor expression level of Fzd8 or Lrp6 was variable in the transiently transfected cells, only cells with similar receptor expression levels were considered (less than 3-times excess of one subunit over the other). The smaller number of trajectories of either Fzd8 or Lrp6 was regarded as the limiting factor and therefore taken as a reference for calculating the heterodimerized/-oligomerized fraction. Oligomerization values were not corrected for the degree of labeling.

Single molecule tracking

Single molecule trajectories were reconstructed using the multi-target tracing (MTT) algorithm [56]. The detected trajectories were evaluated with respect to their step length distribution to determine the diffusion coefficients. For a reliable quantification of local mobilities, we estimated diffusion constants from the displacements with 3 frames (96 ms). Step-length histograms were obtained from all single molecule trajectories and fitted by a two-component model of Brownian diffusion, thus taking into account the intrinsic heterogeneity of protein diffusion in the plasma membrane [50,57,58]. A bimodal probability density function $p(r)$ was used for a nonlinear least square fit of the step-length histogram:

$$p(r)=\sum_i \alpha_i \cdot \frac{r}{\sigma_i^2} e^{(-r^2/2\sigma_i^2)} \text{ and } \sum_i \alpha_i=1; \quad \text{Eqn (1)}$$

where α_i is the percentage of the fraction, $\sigma_i^2=2D_i n\delta t$ contains the diffusion coefficient of each fraction ($n\delta t$ = 96ms). Average diffusion coefficients were determined by weighting the diffusion coefficients with the corresponding fractions.

Single molecule intensity assay

Single molecule intensity distribution of individual diffraction-limited spots was extracted from the first 50 images of the recorded time lapse image sequence, in which photobleaching of dyes was kept below 10% [50]. Oligomerization of receptors was evaluated by fitting the obtained single molecule intensity with a multi-component Gaussian distribution function [59]. To ensure a reliable analysis, monomeric receptors were first distinguished based on the observation that monomers diffused much faster than oligomers. Therefore, the characteristic intensity distribution of monomeric receptor subunits was obtained by tracking of the fast mobile fraction. Fractions of the monomer, dimer, trimer, and higher oligomers were then de-convoluted from the single molecule intensity distribution, presuming that intensities of clusters were multiples of the monomer intensity distribution.

STF and BAR luciferase reporter assays

Immortal cells were seeded in triplicate for each condition in 96-well plates, and stimulated with surrogates, XWnt8, Wnt3a-CM, control proteins, or other treatments for 20–24 hrs. After washing cells with 1xPBS, cells in each well were lysed in 30 μl 1× passive lysis buffer (Promega). 10 μl per well of lysate was assayed using the Dual Luciferase Assay kit (Promega) and normalized to the renilla luciferase signal driven constitutively by the EF1-α promoter to account for cell variability. A375 BAR, SH-SY5Y BAR, L STF and 293 STF cells were plated at a density of 10'000–20'000 cells/well, and treatment was started after 24hrs in fresh medium. A549 BAR cells were plated at a density of 5'000 cells/well in the presence of 2 μM IWP-2 (Calbiochem) to suppress endogenous Wnt secretion, and treatment was started after 48 hrs in fresh medium containing fresh IWP-2.

β-catenin stabilization and Lrp6 phosphorylation assay

To induce β-catenin accumulation, SH-SY5Y BAR cells were treated for 2hrs with scFv-DKK1c, Wnt3a-CM (positive control), B12 (negative control protein), mock-CM (from untransfected L cells, negative control) at 37°C, 5% CO_2. After, cells were washed twice with 1xPBS. For β-catenin stabilization assay, cells were scraped into hypotonic lysis buffer (10 mM Tris-HCl pH 7.4, 0.2 mM MgCl2 supplemented with protease inhibitors), incubated on ice for 10 min, and homogenized using a hypodermic needle. Sucrose and EDTA were added to final concentration of 0.25 M and 1 mM, respectively. For Lrp6 phosphorylation assay, cells were lyzed in RIPA buffer (50 mM Tris pH 8.0, 150 mM NaCl, 0.5 % sodium deoxylate, 1 % Triton X 100), supplemented with protease inhibitor and phosphatase inhibitor for 1 hr at 4C. Lysates were centrifuged at 12,000xg for 1 hr at 4°C. Supernatants were then diluted into SDS sample buffer. For immunoblotting, samples were resolved on a 12% Mini-PROTEAN(R)TGX precast protein gel (Bio-Rad) and transferred to a PVDF membrane. The membranes were cut horizontally approx. at the 64 kDa mark of the SeeBlue plus 2 molecular weight marker (Invitrogen). Upper half of the blot was incubated with anti-β-catenin primary antibody ((D10A8)XP, rabbit, Cell Signaling #8480), Lrp6 antibody ((C47E12), rabbit, Cell Signaling #3395), and P-Lrp6 (S1490) antibody (rabbit, Cell Signaling #2568), and the lower part with the anti-α-tubulin primary antibody (mouse, DM1A, Sigma) in 1xPBS containing 0.1 % Tween-20 and 5 % BSA overnight at 4°C. Blots were then washed, incubated with the corresponding secondary antibodies in the same buffer, before washing and developing using the ECL prime western blotting detection reagent (GE Healthcare).

Kinetic measurements of β-catenin accumulation

To induce β-catenin accumulation, K562 and cells were stimulated for 0, 15, 30, 45, 60, 90, and 120 min with 10 nM scFv-DKK1c, recombinant Wnt3a (R&D Systems), B12 (negative control protein) or plain complete growth medium at 37°C, 5% CO_2. After, cells were washed twice with 1xPBS, fixed with 4% PFA for 10 min at room temperature, and permeabilized in 100% methanol for at least 30 min at −80°C. The cells were than stained with Alexa-647 conjugated anti-β-catenin antibody (L54E2) (Cell Signaling Technology, 1:100 – 1: 50 dilution). Fluorescence was analyzed on an Accuri C6 flow cytometer.

RNA isolation, cDNA synthesis, and qPCR

Total RNA was isolated using either TRIZOL (Invitrogen) or RNeasy plus micro kit (QIAGEN) according to manufacturer's protocols. A total of 2 μg RNA were used to generate cDNA using the RevertAid RT kit (Life Technologies) using oligo(dT)18 mRNA primers (Life Technologies) according to manufacturer's protocol. 12 ng of cDNA per reaction were used. qPCR was performed using SYBR Green-based detection (Applied Biosystems) according to the manufacturer's protocol on a StepOnePlus real-time PCR system (ThermoFisher Scientific). All primers were published, or validated by us. Transcript copy numbers were normalized to GAPDH for each sample, and fold induction compared to control was calculated.

The following gene-specific validated primers were used:

Human Fzd1: F: atcctgtgtgctcctcttttgg, R: gattgcttttctcctcttcttcac

Human Fzd2: F: ctgggcgagcgtgattgt, R: gtggtgacagtgaagaaggtggaag

Human Fzd3: F: tctgtattttgggttggaagca, R: cggctctcattcactatctcttt

Human Fzd4: F: tgggcacttttcggtattc, R: tgcccaccaacaaagacata

Human Fzd5: F: ccatgattctttaaggtgagctg, R: acttattcaagacacaacgatgg

Human Fzd6: F: cgatagcacagcctgcaata, R: acggtgcaagccttattttg

Human Fzd7: F: taccatagtgaacgaagagga, R: tgtcaaaggtgggataaagg

Human Fzd8: F: acccagccccttttcctccatt, R: gtccaccctcctcagccaac

Human Fzd9: F: gctgtgactggaataaacccc, R: gctctgcttacaagaaagactcc

Human Fzd10: F: ctcttctctgtgctgtacacc, R: gtcttggaggtccaaatcca

Mouse Fzd1: F: gcgacgtactgagcggagtg, R: tgatggtgcggatgcggaag[60]

Mouse Fzd2: F: ctcaaggtgccgtcctatctcag, R: gcagcacaacaccgaccatg[60]

Mouse Fzd3: F: ggtgtcccgtggcctgaag, R: acgtgcagaaaggaatagccaag[60]

Mouse Fzd4: F: gacaactttcacgccgctcatc, R: caggcaaacccaaattctctcag[60]

Mouse Fzd5: F: aagctgccttcggatgacta, R: tgcacaagttgctgaactcc[60]

Mouse Fzd6: F: tgttggtatctctgcggtcttctg, R: ctcggcggctctcactgatg[60]

Mouse Fzd7: F: atatcgcctacaaccagaccatcc, R: aaggaacggcacggaggaatg[60]

Mouse Fzd8: F: gttcagtcatcaagcagcaaggag, R: aaggcaggcgacaacgacg[60]

Mouse Fzd9: F: atgaagacgggaggcaccaatac, R: tagcagacaatgacgcaggtgg[60]

Mouse Fzd10: F: atcggcacttccttcatcctgtc, R: tcttccagtagtccatgttgag[60]

Human Axin2: F: ctccccaccttgaatgaaga, R: tggctggtgcaaagacatag

Human GAPDH: F: tgaaggtcggagtcaacgga, R: ccattgatgacaagcttcccg

Mouse GAPDH: F: ccccaatgtgtccgtcgtg, R: gcctgcttcaccaccttct

Osteogenic differentiation assay

Differentiation of C3H10T1/2, and human and mouse primary MSCs were performed essentially as described previously [61]. Briefly, ~10,000 cells/cm^2 were plated in normal culture medium (αMEM + FBS + P/S), and allowed to adhere overnight. The following day, the medium was replaced with osteogenic medium (αMEM, 10 % FBS, 1 % P/S, 50 μg/mL ascorbic acid, 10 mM β-glycerol phosphate (βGP), and replaced every other day. To determine ALP enzymatic activity, cells were fixed for 10 minutes with 10% formalin in PH7 PBS, before incubation in NBT-BCIP solution (1-Step(tm) NBT/BCIP Substrate Solution (Thermo Fisher Scientific, Cat # 34042) for 30 minutes. qPCRs were done with the SYBR method using the following primers:

hACTB-F:GTTGTCGACGACGAGCG

hACTB-R:GCACAGAGCCTCGCCTT

hALP-F:GATGTGGAGTATGAGAGTGACG

hALP-R:GGTCAAGGGTCAGGAGTTC

mALP-F:AAGGCTTCTTCTTGCTGGTG

mALP-R:GCCTTACCCTCATGATGTCC

mActin-F:GGAATGGGTCAGAAGGACTC

mActin-R:CATGTCGTCCCAGTTGGTAA

mCol2a1_F:GTGGACGCTCAGGAGAAACA

mCol2a1_R:TGACATGTCGATGCCAGGAC

Human organoid culture assay

P26N, normal adult human colon organoids, were established from a tumor-free colon segment of a patient diagnosed with CRC as described[18,62,63]. CFTR-derived colorectal organoids were obtained from a patient at Wilhelmina Children's Hospital WKZ-UMCU. Informed consent for the generation and use of these organoids for experimentation was approved by the ethical committee at University Medical Center Utrecht (UMCU)(TcBio #14-008). Human stomach organoids, derived from normal corpus and pylorus, were from patients that underwent partial or total gastrectomy at the University Medical Centre Utrecht (UMCU) and were established as described[19,64,65]. Pancreas organoids were obtained from the healthy part of the pancreas of patients undergoing surgical resection of a tumor at the University Medical Centre Utrecht Hospital (UMC) and were established as described[66,67]. The liver organoids were derived from freshly isolated normal liver tissue from a metastatic CRC-patient who presented at the UMC hospital (Ethical approval code is TCBio #14-007) and were established as described[20,68].

For the performance of 3D cultures, Matrigel (BD Biosciences) was used and overlaid with a liquid medium consisting of DMEM/F12 advanced medium (Invitrogen), supplemented with additional factors as outlined below. 2% RSPO3-CM (produced via the r-PEX protein expression platform at U-Protein Express BV, Utrecht, the Netherlands), mWnt3a-conditioned medium (50%, produced using stably transfected L cells in the presence of

DMEM/F12 advanced medium supplemented with 10% FBS), and Wnt- and Wnt/RSPO2-surrogates at different concentrations were added as indicated. Single-cell suspensions of normal human organoids were cultured in triplicate in round-bottom 96-well plates in order to perform a cell viability test using Cell Titer-Glo 3D (Promega). Briefly, organoids were trypsinized to single cell suspension and plated in 100 µl medium in the presence of the different reagents. 3 µM IWP-2 was added to inhibit endogenous Wnt lipidation and secretion. After 12 days, 100 µl of Cell Titer-Glo 3D was added, plates were shaken for 5 minutes, incubated for an additional 25 minutes and centrifuged prior to luminescence measurement.

In vivo experiments

All animal experiments were conducted in accordance with procedures approved by the IACUC at Stanford University. Experiments were not randomized, the investigators were not blinded, and all samples/data were included in the analysis. Group sample sizes were chosen based on 1) previous experiments, 2) in order to perform statistics analysis, and 3) logistical reasons with respect to full study size, in order to accommodate all groups. Adenoviruses (E1- and E3- deleted, replication deficient) were constructed to express scFv-DKK1c or scFv-DKK1c-RSPO2 with an N-terminal signal peptide and C-terminal 6 × histidine-tag (Ad scFv-DKK1c or Ad scFv-DKK1c-RSPO2), respectively. Adenoviruses expressing mouse IgG 2α Fc (Ad Fc), human RSPO2-Fc fusion protein (Ad RSPO2-Fc) and mouse Wnt3a (Ad Wnt3a) were constructed and described in the companion paper by Yan et al. The adenoviruses were cloned, purified by CsCl gradient, and titered as previously described [69]. Adult *C57Bl*/6J mice (Jackson Laboratory, ME, USA) between 8–10 weeks old were injected intravenously with a single dose of adenovirus at between 1.2×10^7 pfu to 6×10^8 pfu per mouse in 0.1 mL PBS. Serum expression of Ad scFv-DKK1c or Ad scFv-DKK1c-RSPO2 were confirmed by immunoblotting using mouse anti-6 × His (Abcam ab18184, 1:2000) or rabbit anti-6 × His (Abcam ab9108, 1:1000), respectively. All *e*xperiments used *n* = 4 mice per group and repeated at least twice.

qRT-PCR on liver samples were performed as following. Total cDNA was prepared from each liver sample using Direct-Zol RNA miniprep kit(Zymo Research) and iScript Reverse Transcription Supermix for RT-qPCR(BIO-RAD). Gene expression was analyzed by −ΔΔCt or Fold change ($2^{(-\Delta\Delta Ct)}$). Unpaired Student's t test (two tailed) was used to analyze statistical significance. Primers for Axin2 and Cyp2f2 were previously published[70]. Additional primers used were listed as below:

scFv-DKK1c (ScFv-DKK1 junction)

ScFv-Dkk1 F: TCAAGTACGTGTTCGCCAA

ScFv-Dkk1 R: TCAGAGGACCTCAGGCACA

scFv-DKK1c-RSPO2 (DKK1-RSPO2 junction)

Dkk1-Rspo2 F: ATCATCAGGCCTCCAACT

Dkk1-Rspo2 R: CAACCCTTGCAAATGGGA

Rspo2 hFc (Rspo2-hFc junction)

Rspo2-hFc F: TTGCATAGAGGCCGTTGCT

Rspo2-hFc R: CCATTCGCTCCAATGACCAA

mouse Glns (GS)

mGlns F: ATGCAGATAGGGTGACCACT

mGlns R: GTCCATTTGCAGGAAATGGC

mouse Wnt3a

mWnt3a F: TACCTCTTAGTGCTCTGCAG

mWnt3a R: CTGAGTGCTCAGAGAGGAGT

mouse Axin2:

mAxin2 F: GCAGGAGCCTCACCCTTC

mAxin2 R: TGCCAGTTTCTTTGGCTCTT

mouse Cyp2f2

mCyp2f2 F: CCGGAACTTTGGAGGCATGAA

mCyp2f2 R: GGTCATCAGCAGGGTATCCAT

For the parabiosis experiment, age and gender-matched *C57Bl*/6J mice were housed together for at least 2 weeks before surgery. At 2 days before surgery, the “donor” mice were injected intravenously with a single dose of adenovirus at between 1.2×10^7 pfu to 6×10^8 pfu per mouse in 0.1 mL PBS and were separated from the “recipient” mice until surgery. The parabiosis surgery was performed as described previously[71]. The establishment of shared circulation was confirmed at day 5 after surgery by presence of adenovirus-expressed proteins in the serum of both donors and recipients.

Histological analysis and Immunofluorescence

Mouse livers were harvested and fixed in 4% paraformaldehyde. 5 μm paraffin-embedded sections were stained with the following antibodies following citrate antigen retrieval and blocking with 10% normal goat serum: mouse anti-glutamine synthetase antibody (Millipore #MAB302, 1:200), mouse anti-PCNA (BioLegend #307902, 1:200), and rabbit anti-HNF4α (Cell Signaling #3113S, 1:500). The immunostained tissue sections were analyzed and images were captured on a Zeiss Axio-Imager Z1 with ApoTome attachment.

Extended Data

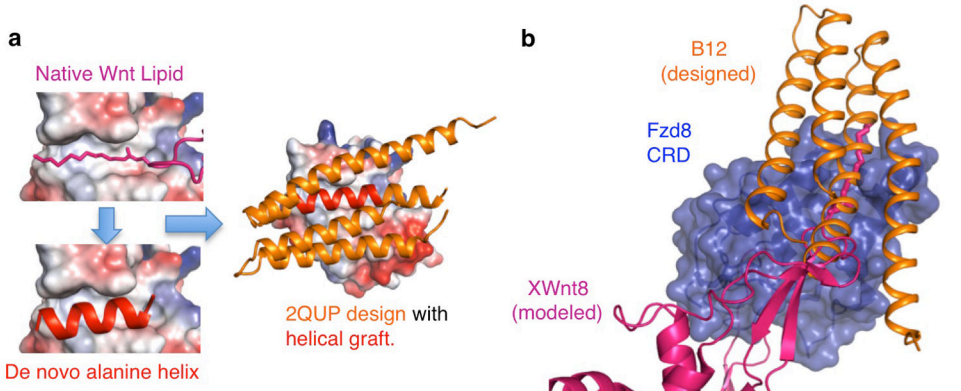

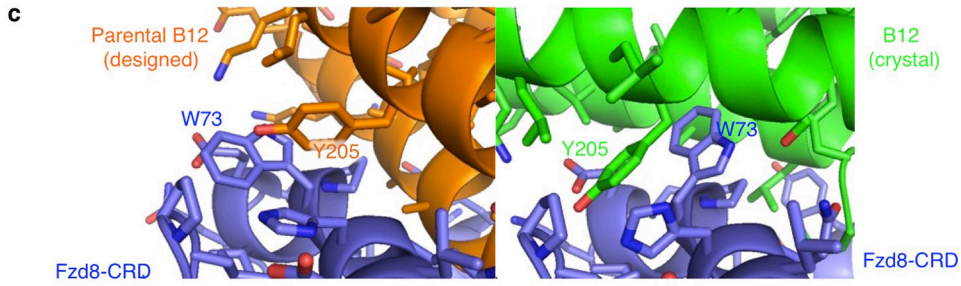

d

Position	147	169	174	177	178	184	206	235	238	239	240
Parental B12 AA	K	A	A	A	A	K	K	L	R	I	Y
Enriched AA	I	V	L/T	L	Q	P	L	T/I	S	G/V	P
Selected AA	**I**	**V**	**T**	**L**	**Q**	**P**	**L**	**T**	R	**V**	Y

Extended Data Figure 1. De novo design and engineering of B12

a, Design strategy of a Fzd8-CRD specific binding domain. **b,** Designed binding of B12 (orange) to the Fzd8-CRD (blue), with XWnt8 and Wnt lipid (purple) modeled onto the structure to highlight competitive binding modes. Residues outside of the 'lipid groove helix' make Fzd8-specific contacts to promote specificity. **c,** Comparison between the designed (left panel) and observed conformation (right panel). **d,** Affinity maturation of parental B12 by yeast cell surface display identified enriched point mutations which were assembled in a degenerate library and selected to yield the final, optimized B12.

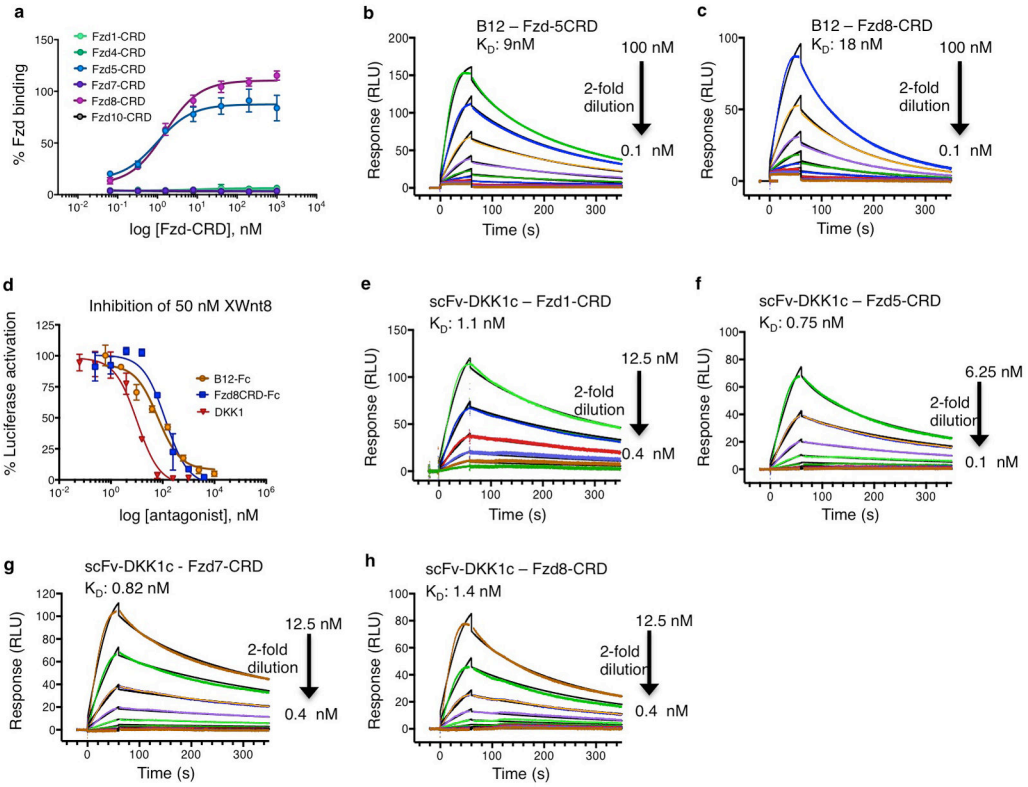

Extended Data Figure 2. Fzd-CRD binding characterization of B12 and scFv

a, Binding specificity of the B12-Fzd-CRD interaction determined by yeast cell surface titration. B12 was displayed on yeast and binding of monomeric Fzd-CRDs fluorescently labeled with SAV-Alexa647 was detected by flow cytometry. Error bars represent S.D. of n=3 technical replicates from one of 2 representative experiments. **b–c,** Binding affinity of the B12-Fzd5/8-CRD interaction determined by surface plasmon resonance. Fzd5/8-CRDs were immobilized on a streptavidin chip, and B12 was flown through as analyte. **d,** Inhibition of XWnt8 induced signaling in A549 cells as measured by BAR luciferase reporter assay. Error bars represent S.D. of n=3 technical replicates from one of 2 representative experiments. **e–h,** Binding affinity of the scFv-DKK1c – Fzd1, Fzd5, Fzd7, Fzd8-CRD interaction determined by surface plasmon resonance. Fzd-CRDs were immobilized on a streptavidin chip, and scFv-DKK1c was flown through as analyte.

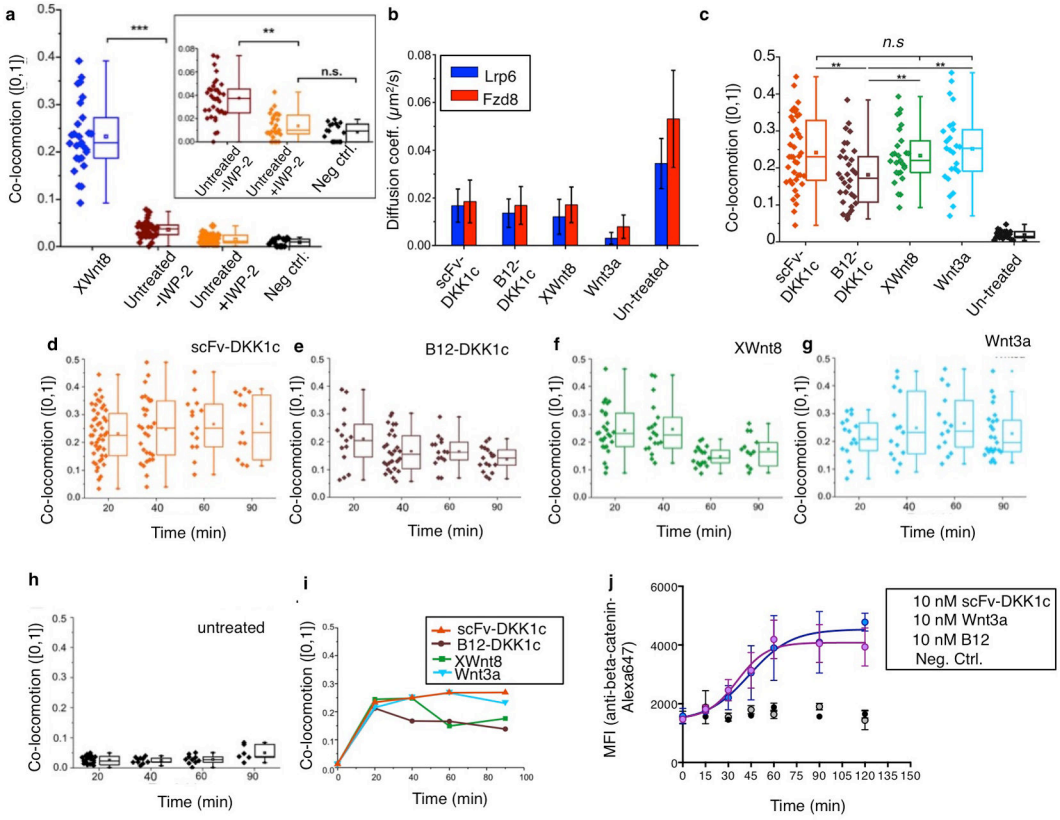

Extended Data Figure 3. Co-locomotion analysis of Lrp6 and Fzd8 induced by Wnt and Wnt surrogate

a, Dimer-/oligomerization of Lrp6 and Fzd8 quantified by co-locomotion of both receptors under different conditions. Negative control (black) is the dimerization of Dy649-labeled Fzd8 and a TMR-labeled model transmembrane protein, HaloTag-maltose binding protein-TMD, co-expressed in HeLa cells. Addition of 2 μM IWP-2 for 20 h reduced the receptor dimerization to the background level of the negative control (inset). Receptor dimerization induced by XWnt8 was used as a positive control (blue). The box chart represents measurements of >18 individual cells for each condition. ***p<0.001, **p<0.01, t-test. **b,** Diffusion coefficients of Lrp6 and Fzd8 in the absence or presence of 100 nM Wnt surrogates and control Wnts. Error bars represent S.D. from >25 individual cells. **c,** Co-locomoting Lrp6/Fzd8 measured within 30 min after the addition of 100 nM scFv-DKK1c, B12-DKK1c, XWnt8 and Wnt3a, or without treatment. The box chart represents measurements of individual cells for each condition (**, p<0.01, t-test). scFv-DKK1c (n=40), B12-DKK1c (n=32), XWnt8 (n=27), Wnt3a (n=25), and without treatment (n=28). **d–i**, Dimer-/oligomerization of Lrp6 and Fzd8 as a function of time after addition of 100 nM scFv-DKK1c (**d**), B12-DKK1c (**e**), XWnt8 (**f**) and Wnt3a (**g**). More than 12 individual cells were evaluated for each condition. **h,** Time course control of untreated cell. **i,** Summarized representation of time course of Lrp6/Fzd8 complex formation. **j,** Kinetics of β-catenin accumulation in K562 cells after stimulation with 10 nM scFv-DKK1c, recombinant Wnt3a, B12, or basal conditions only (complete growth medium). Error bars represent S.D. of n=3 technical replicates from one of 2 representative experiments.

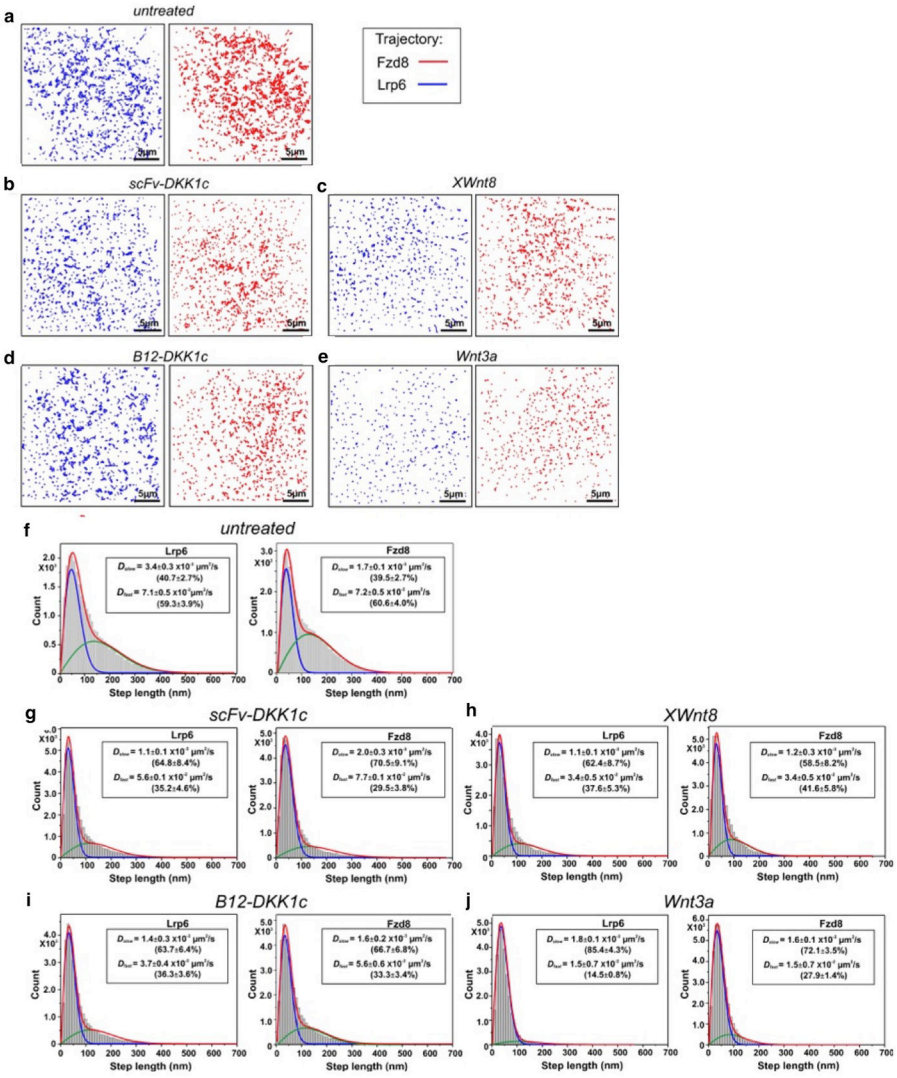

Extended Data Figure 4. Single molecule trajectories and step length analysis of Lrp6 and Fzd8 under different conditions

a–e, Single molecule trajectories obtained for Lrp6 and Fzd8 in the plasma membrane of representative HeLa cells under different conditions. Trajectories were obtained by single molecule tracking of the dye-labeled Lrp6 (blue) and Fzd8 (red) in the dual-color time-lapse single molecule images within 150 frames. Fast diffusion results into spread-out trajectories (prominent in panel a) while slow diffusion leads to dot-like trajectories (prominent in panel e). **f–j,** Step length histogram analyses for determining diffusion coefficients of Lrp6 and Fzd8, shown for representative individual cells under different conditions. Step lengths for a time lapse of 3 frames (96 ms) were calculated from trajectories shown in (a–e). According to Eqn S1, a two component model comprising a slow (blue) and a fast (green) fraction was used for fitting the histograms. Inset: diffusion coefficient and the corresponding fraction in percentage (in bracket).

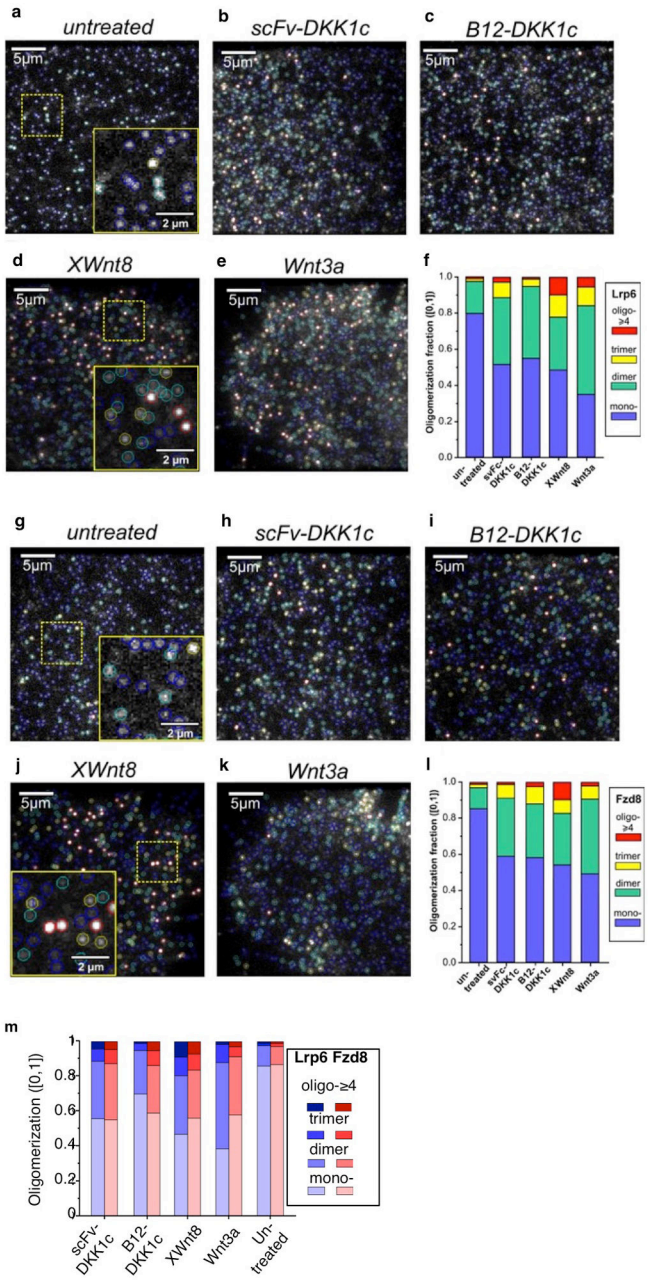

Extended Data Figure 5. Single molecule intensity analysis of Lrp6 and Fzd8 under different conditions

Single molecule intensity analysis for quantifying Lrp6 (**a–f**) and Fzd (**g–l**) oligomerization in representative cells under different conditions. Raw images of (**a, g**) without treatment, (**b, h**) scFv-DKK1c, (**c, i**) B12-DKK1c, (**d, j**) XWnt8 and (**e, k**) Wnt3a. Based on their intensities, individual diffraction-limited spots in the raw images were classified as monomers (blue circle), dimers (green circle), trimers (yellow circle) and higher oligomers (red circle), respectively. (**f, l, m**) Different oligomer fractions summarized as the ratio of the classified species number to the total number of detected diffraction-limited spots. More than 7200 single complex intensities were examined for each condition.

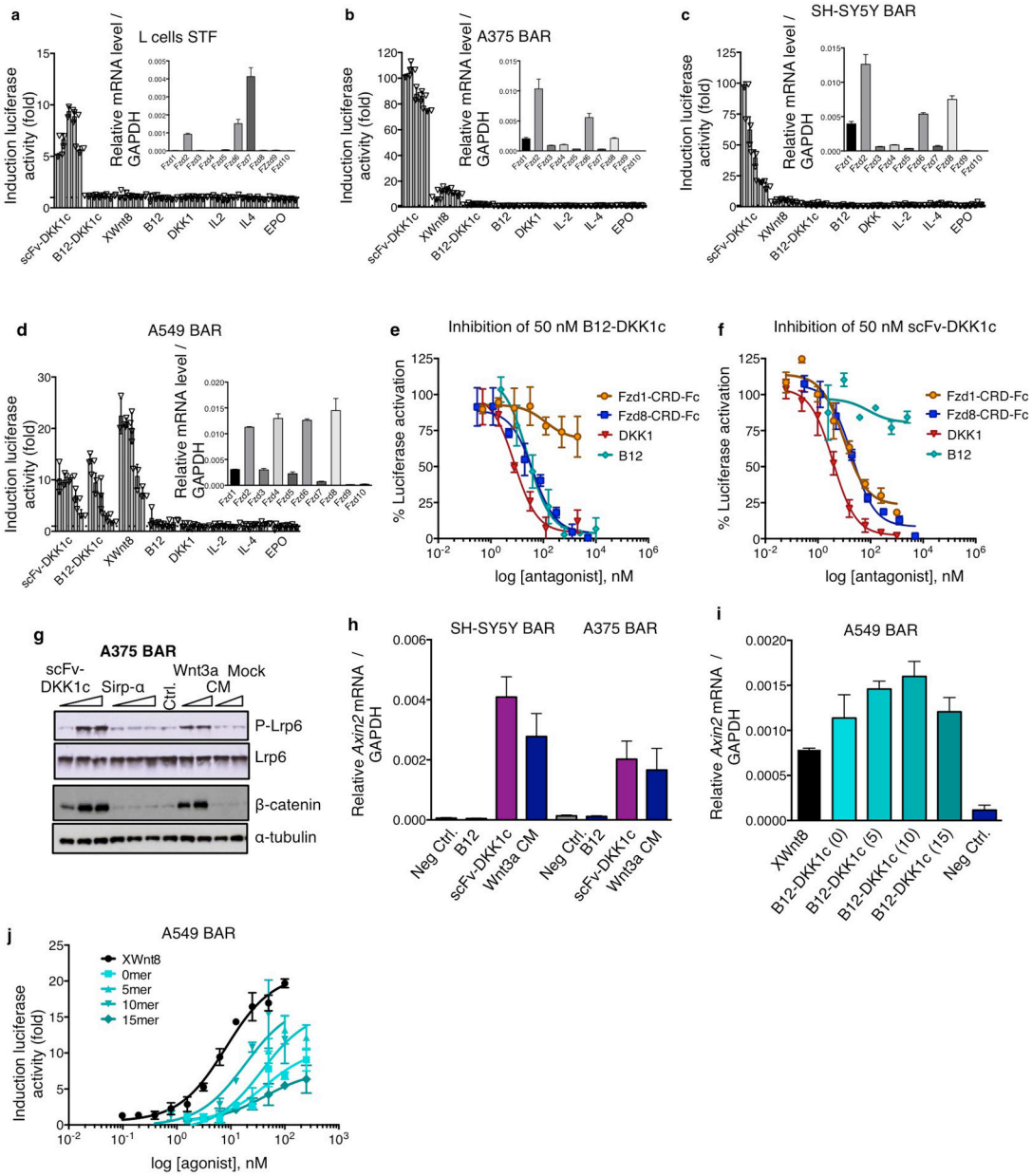

Extended Data Figure 6. Fzd-specific activation of canonical Wnt signaling by Wnt surrogates

a–d, Activation of Wnt pathway by decreasing concentration of scFv-DKK1c, B12-DKK1c, XWnt8 or negative control proteins B12, DKK1, IL-2, IL-4 and EPO assayed by the BAR and STF reporters in (a) L cells (50-3 nM)**,** (b) A375 cells (250-15 nM), (c) SH-SY5Y cells (250-15 nM), and (d) A549 cells (100–1 nM). Error bars represent S.D of n=3 technical replicates from one of 2 representative experiments. The relative quantities of human Fzd mRNA in the relative cell lines determined by qRT-PCR are shown as insets, error bars represent S.D. of n=3 technical replicates. **e–f**, Selective inhibition of B12-DKK1c and scFv-DKK1c activity in A549 cells by B12, DKK1, Fzd1-CRD-Fc and Fzd8-CRD-Fc assayed by the BAR reporter, correlates with binding specificity. Error bars represent S.D. of n=3 technical replicates. **g,** Immunoblot analysis of Lrp6 phosphorylation and β-catenin

accumulation in A375 BAR cells treated with scFv-DKK1c and hSirpα (0.1, 10, 50 nM), Wnt3a-CM and mock CM (30, 50 %). **h,** *Axin2* transcription relative to GAPDH in SH-SY5Y BAR and A375 BAR cells treated with 50 nM scFv-DKK1c, B12 (negative control), and 30 % Wnt3a-CM analyzed by qRT-PCR. Error bars represent the S.D. of biological triplicates performed in technical triplicates (n=9). **i,** *Axin2* transcription relative to GAPDH in A549 BAR cells treated with 50 nM B12-DKK1c variants, and XWnt8 analyzed by qRT-PCR. Error bars represent S.D. of biological triplicates performed in technical triplicates (n=9). **j**, Activation of Wnt signaling with distinct amplitudes by XWnt8 and B12-DKK1c variants assayed by the BAR reporter in A549 cells. Error bars represent S.D. of n=3 technical replicates from one of 3 representative experiments.

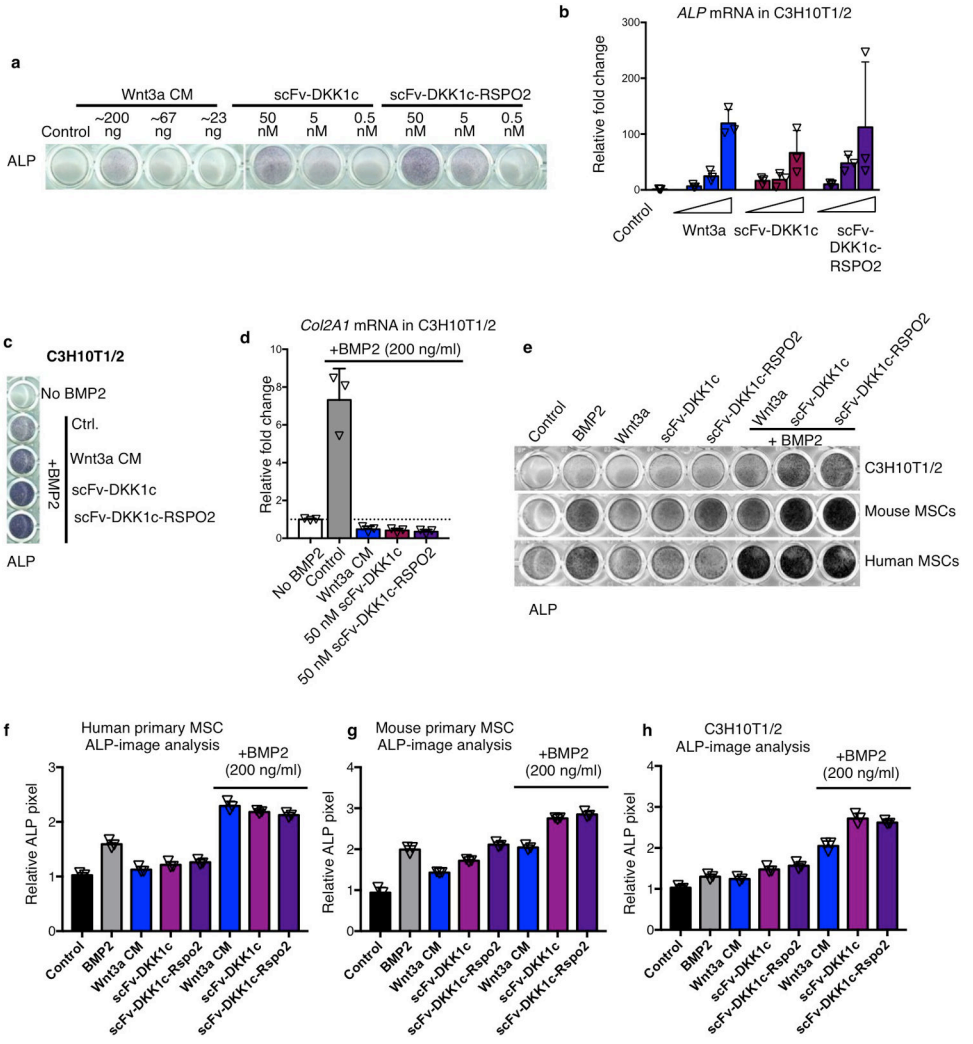

Extended Data Figure 7. Wnt surrogates enhance up-regulation of ALP in MSCs

Up-regulation of ALP assessed by the cell surface enzymatic activity with the ALP substrate NBT/BCIP (**a**), and qRT-PCR of mRNA levels (**b**) in C3H10T1/2 cells treated for 4 days with increasing concentration of Wnt3a CM, scFv-DKK1c (0.5, 5, 50 nM) and scFv-DKK1c-RSPO2 (0.5, 5, 50 nM) in osteogenic media. **c**, Induction of ALP in C3H10T1/2

cells treated with Wnt3a CM, 50 nM scFv-DKK1c and 50 nM scFv-DKK1c-RSPO2 in the presence of 200 ng/ml BMP2 in osteogenic media for 10 days, assayed by cell surface ALP enzymatic activity with the ALP substrate NBT/BCIP. **d**, Relative changes of *collagen 2A1* mRNA levels, an early marker of chondrogenesis, in C3H10T1/2 treated with Wnt3a CM, scFv-DKK1c and scFv-DKK1c-RSPO2 in the presence of BMP2 in osteogenic media for 4 days. **e,** Up-regulation of ALP cell surface enzymatic activity assessed with the ALP substrate NBT/BCIP in C3H10T1/2, mouse primary MSCs, and human primary MSCs treated for 3 days with Wnt3a CM, 50 nM scFv-DKK1c, and 50 nM scFv-DKK1c-RSPO2 in osteogenic media in the presence and absence of 200 ng/ml BMP2. **f–h**, Pixel quantification of images in (e) using ImageJ. Error bars represent S.D. of n=3 technical replicates from one of 3 (C3H10T1/2 and human MSCs) and 1 (mMSCs) representative experiments.

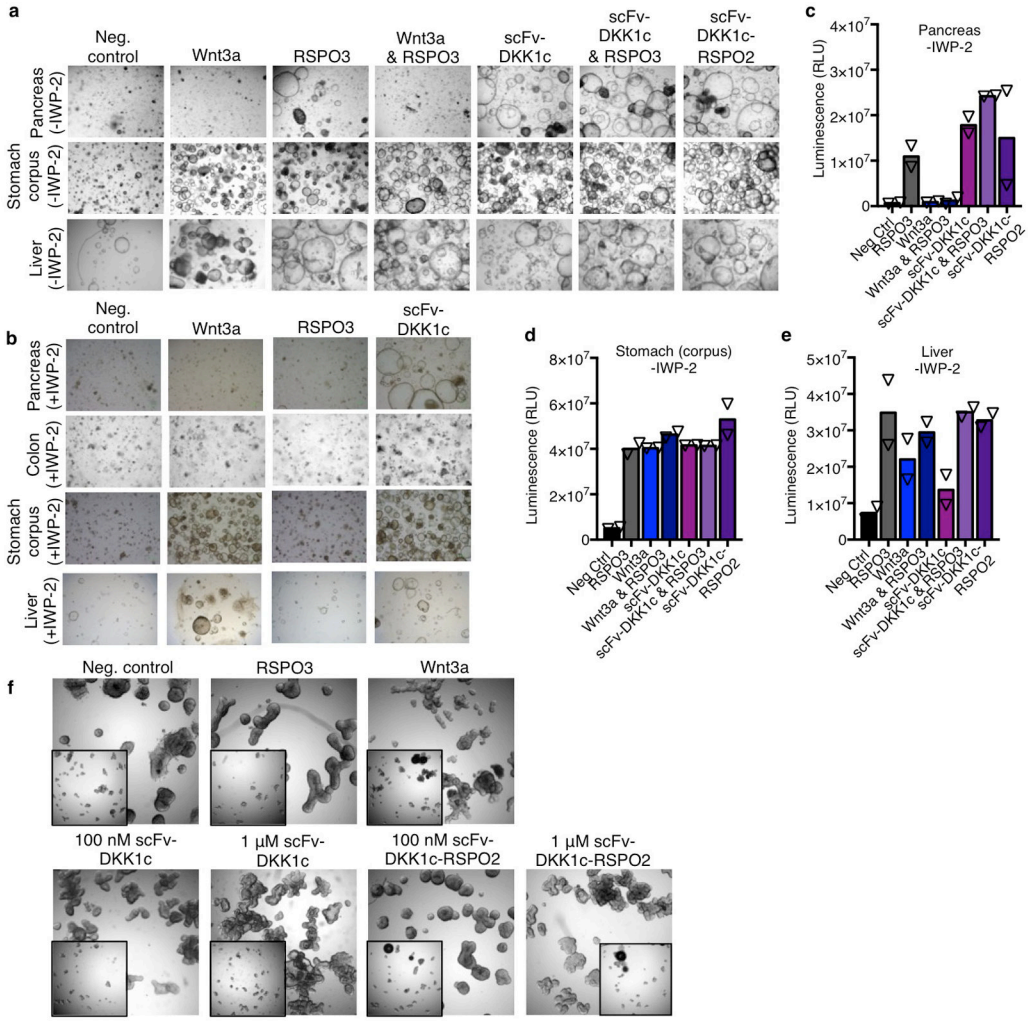

Extended Data Figure 8. Activity of Wnt surrogates on human organoid cultures in vitro

a–b, Representative bright-field images of organoids of human pancreas, stomach (corpus), and liver expanded for 12 days in the absence (a) or presence (b) of 3 µM IWP-2 in basal media (as elaborated in Supplementary Info Table 2), supplemented with 50 % Wnt3a-CM,

2 % RSPO3-CM, 200 nM scFv-DKK1c and 200 nM scFv-DKK1c-RSPO2, or combinations thereof as indicated. **c–e**, Quantification of cell proliferation by luminescence. Bars represent mean of n=2 technical replicates from one of 3 (colon), 2 (liver and pancreas) and 1 (stomach) representative experiments. **f**, Representative bright-field images of colon organoids from a cystic fibrosis patient with characteristic budded morphology owing to mutations in the ion channel CFTR, grown in expansion media with 50 % Wnt3a-CM, 2 % RSPO3-CM, 100 and 1000 nM scFv-DKK1c and 100 and 1000 nM scFv-DKK1c-RSPO2, or combinations thereof as indicated.

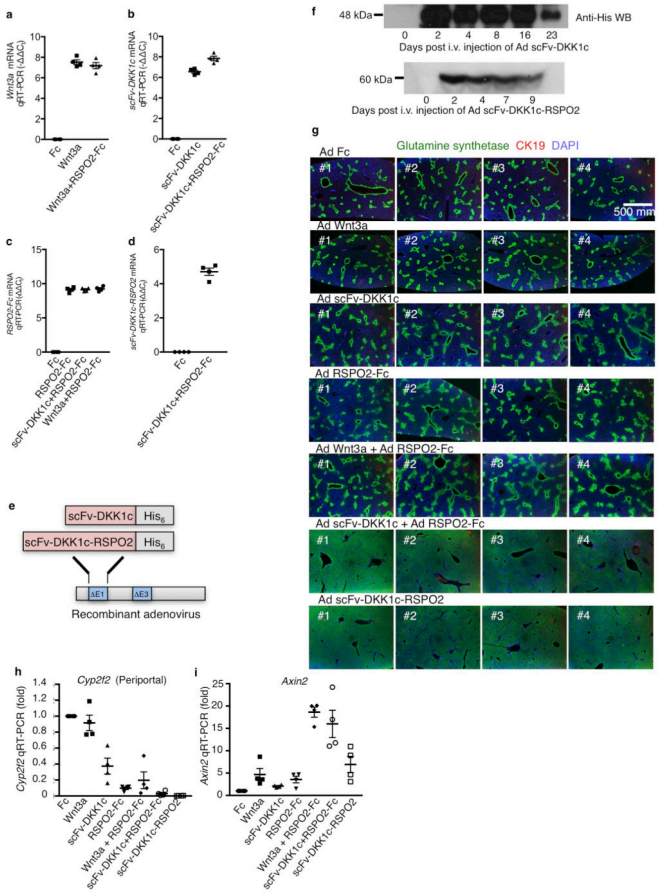

Extended Data Figure 9. Wnt surrogate activate Wnt signaling in vivo and alter Wnt-driven hepatic zonation

a–d, qRT-PCR validation of adenoviral transgene expression in mouse livers 7 days after i.v. injection with Ad Wnt3a, scFv-DKK1c, RSPO2-Fc or scFv-DKK1c-RSPO2 from the same experiment as in (g). N=4 mice per condition. **e**, Schematic representation of Ad scFv-DKK1c and Ad scFv-DKK1c constructs for adenoviral transgene expression. **f**, Detection of scFv-DKK1c and scFv-DKK1c-RSPO2 in mice sera by Western blot at the indicated days after adenovirus injection. **g**, Images from biological replicate mice depicting effects of adenoviral expression of various Wnt agonists on liver zonation from Fig. 4a–b. Mice (n=4/condition) received single i.v. injection of adenovirus expressing Fc (2.5×10^8 pfu), scFv-DKK1c (1.2×10^7 pfu), Wnt3a (1.2×10^7 pfu), RSPO2-Fc (2.5×10^8 pfu), scFv-DKK1c-

RSPO2, or combinations. In all cases the total virus dose was increased to a total of 2.5 × 10^8 pfu by Ad Fc as filler. After 7 days, liver was analyzed for GS expression by immunofluorescence. Anti-CK19 Immunofluorescence was performed to mark portal areas. Each panel is a representative image from a different mouse. **h,i,** qRT-PCR analysis of periportal marker *Cyp2f2* (h) and Wnt target gene *Axin2* (i) of livers from mice that received adenoviruses expressing mouse IgG Fc (Fc), mouse Wnt3a, scFv-DKK1c, human RSPO2-Fc, Wnt3a + RSPO2-Fc, scFv-DKK1c + RSPO2-Fc or scFv-DKK1c-RSPO2, 7 days post adenovirus injection (n=4 mice/group). Error bars indicate S.E. of biological replicates.

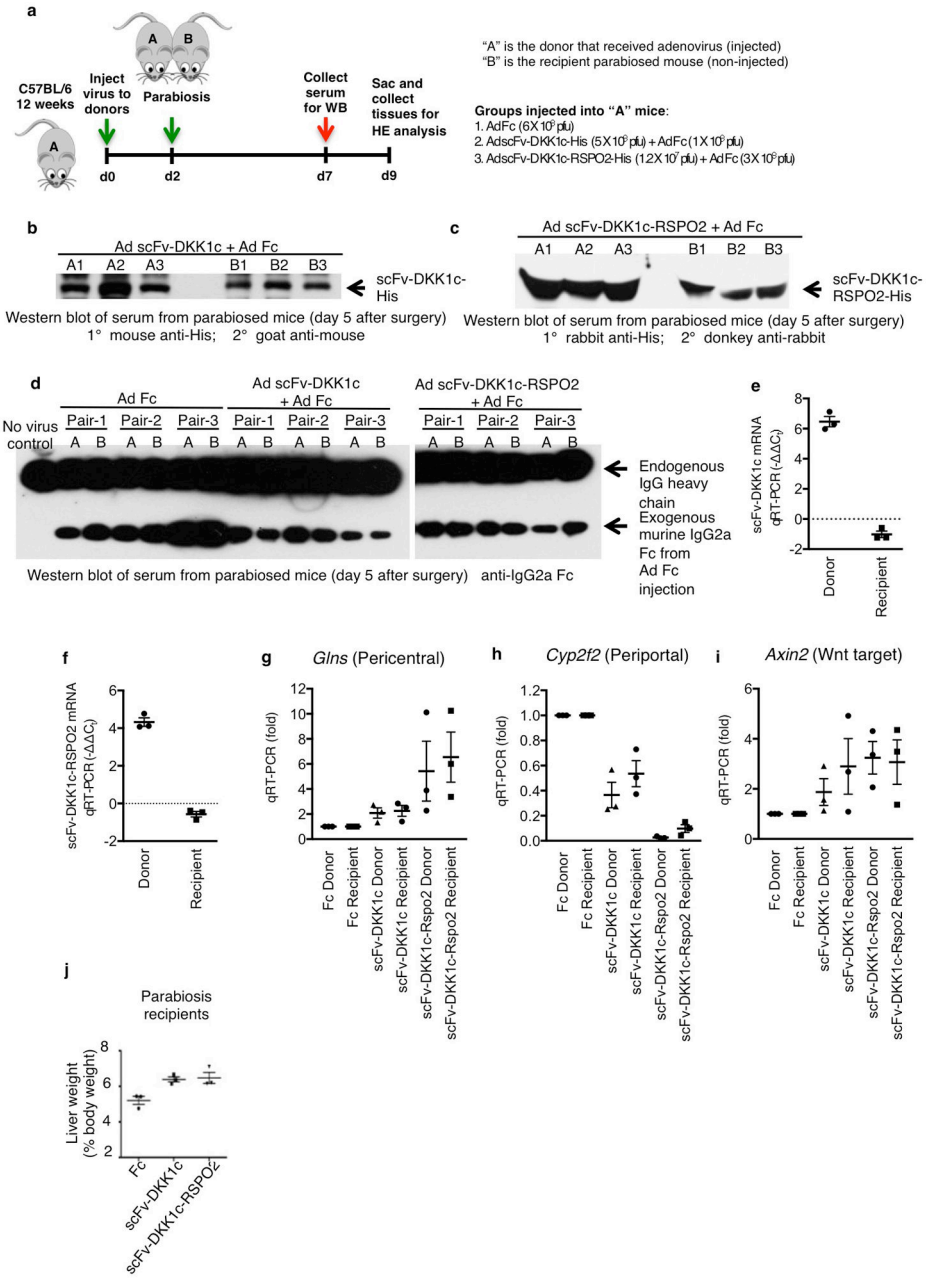

Extended Data Figure 10. Wnt surrogate enhance hepatocyte proliferation

a, Scheme depicting parabiosis experiment design. Age and gender-matched mice were selected and housed together. The donors received adenovirus injection i.v. of either (1) Ad Fc, (2) Ad scFv-DKK1c-His + Ad Fc or (3) Ad scFv-DKK1c-RSPO2 + Ad Fc with liver infection of the donors. Two days later, parabiosis surgery was performed to surgically pair the adenovirus injected donor mice with the recipient mice that did not receive adenovirus injection. Ad Fc was deliberately added to all treatment groups as a tracer to monitor successful establishment of cross-circulation (see b, below). **b–d**, Detection of scFv-DKK1c (b), scFv-DKK1c-RSPO2 (c) or the tracer Fc (d) in the serum of recipients and donor mice 5 days after parabiosis by Western blotting. **e–f**, Liver qRT-PCR validation of adenoviral transgene expression from donor and recipient mice at 7 days surgery (9 days after adenoviral injection) for scFv-DKK1c or scFv-DKK1c-RSPO2. Note absence of transgene expression in the recipient livers. **g–i**, Analysis of livers by qRT-PCR for *Glns* (gene name for Gs), *Cyp2f2* and *Axin2* mRNA with induction of *Glns* and *Axin2* and repression of *Cyp2f2* in both donors and recipients. **j,** Liver weight of recipients 7 days after parabiosis surgery. N=3 mice per condition. Error bars indicate S.E. of biological replicates.

Supplementary Material

Refer to Web version on PubMed Central for supplementary material.

Acknowledgments

We thank the staff of the Advanced Light Source (ALS), Lawrence Berkeley National Laboratory, for support and access to beamline 8.2.2, and Pauline Chu from the Department of Comparative Medicine Animal Histology Service Center for sample preparation. This work was supported by NIH R01 GM097015 (to K.C.G), K08DK096048 (to K.S.Y), U01 DK085527 (to C.J.K.), U19 AI116484 (to C.J.K.), U01 CA176299 (to C.J.K); DFG SFB 944 (to J.P.); Burroughs Wellcome Fund CAMS (to K.S.Y.); the Stinehart/Reed Foundation (to K.C.G); the Ludwig Foundation (K.C.G); the Howard Hughes Medical Institute (to K.C.G.,D.B.), the European Union's Horizon 2020 research and innovation program under grant agreement No 668294 (to H.C.), and the NWO translational Adult Stem Cell Research grant 40-41400-98-1108 (to H.C.). Structure factors and coordinates are being processed for submission to the Protein Data Bank and will be released upon publication.

References

1. Clevers H, Nusse R. Wnt/beta-catenin signaling and disease. Cell. 2012; 149:1192–1205. DOI: 10.1016/j.cell.2012.05.012 [PubMed: 22682243]
2. Willert K, et al. Wnt proteins are lipid-modified and can act as stem cell growth factors. Nature. 2003; 423:448–452. [pii]. DOI: 10.1038/nature01611nature01611 [PubMed: 12717451]
3. Takada R, et al. Monounsaturated fatty acid modification of Wnt protein: its role in Wnt secretion. Developmental cell. 2006; 11:791–801. S1534-5807(06)00455-2 [pii]. DOI: 10.1016/j.devcel.2006.10.003 [PubMed: 17141155]
4. Janda CY, Waghray D, Levin AM, Thomas C, Garcia KC. Structural basis of Wnt recognition by Frizzled. Science. 2012; 337:59–64. DOI: 10.1126/science.1222879 [PubMed: 22653731]
5. Cong F, Schweizer L, Varmus H. Wnt signals across the plasma membrane to activate the beta-catenin pathway by forming oligomers containing its receptors, Frizzled and LRP. Development. 2004; 131:5103–5115. DOI: 10.1242/dev.01318 [PubMed: 15459103]
6. Holmen SL, Robertson SA, Zylstra CR, Williams BO. Wnt-independent activation of beta-catenin mediated by a Dkk1-Fz5 fusion protein. Biochemical and biophysical research communications. 2005; 328:533–539. DOI: 10.1016/j.bbrc.2005.01.009 [PubMed: 15694380]
7. Liu G, Bafico A, Aaronson SA. The mechanism of endogenous receptor activation functionally distinguishes prototype canonical and noncanonical Wnts. Molecular and cellular biology. 2005; 25:3475–3482. DOI: 10.1128/MCB.25.9.3475-3482.2005 [PubMed: 15831454]

8. Mulligan KA, et al. Secreted Wingless-interacting molecule (Swim) promotes long-range signaling by maintaining Wingless solubility. Proceedings of the National Academy of Sciences of the United States of America. 2012; 109:370–377. DOI: 10.1073/pnas.1119197109 [PubMed: 22203956]

9. Gurney A, et al. Wnt pathway inhibition via the targeting of Frizzled receptors results in decreased growth and tumorigenicity of human tumors. Proceedings of the National Academy of Sciences of the United States of America. 2012; 109:11717–11722. DOI: 10.1073/pnas.1120068109 [PubMed: 22753465]

10. Ahn VE, et al. Structural basis of Wnt signaling inhibition by Dickkopf binding to LRP5/6. Developmental cell. 2011; 21:862–873. DOI: 10.1016/j.devcel.2011.09.003 [PubMed: 22000856]

11. Bourhis E, et al. Reconstitution of a Frizzled8-Wnt3a-LRP6 signaling complex reveals multiple Wnt and Dkk1 binding sites on LRP6. The Journal of biological chemistry. 2010:M109.092130. [pii].

12. Bilic J, et al. Wnt induces LRP6 signalosomes and promotes dishevelled-dependent LRP6 phosphorylation. Science. 2007; 316:1619–1622. DOI: 10.1126/science.1137065 [PubMed: 17569865]

13. Wilmes S, et al. Receptor dimerization dynamics as a regulatory valve for plasticity of type I interferon signaling. The Journal of cell biology. 2015; 209:579–593. DOI: 10.1083/jcb.201412049 [PubMed: 26008745]

14. Hao HX, et al. ZNRF3 promotes Wnt receptor turnover in an R-spondin-sensitive manner. Nature. 2012; 485:195–200. DOI: 10.1038/nature11019 [PubMed: 22575959]

15. Zhong Z, Ethen NJ, Williams BO. WNT signaling in bone development and homeostasis. Wiley interdisciplinary reviews. Developmental biology. 2014; 3:489–500. DOI: 10.1002/wdev.159 [PubMed: 25270716]

16. Salazar VS, Ohte S, Capelo LP, Gamer L, Rosen V. Specification of osteoblast cell fate by canonical Wnt signaling requires Bmp2. Development. 2016

17. Kretzschmar K, Clevers H. Organoids: Modeling Development and the Stem Cell Niche in a Dish. Developmental cell. 2016; 38:590–600. DOI: 10.1016/j.devcel.2016.08.014 [PubMed: 27676432]

18. Sato T, et al. Single Lgr5 stem cells build crypt-villus structures in vitro without a mesenchymal niche. Nature. 2009; 459:262–265. DOI: 10.1038/nature07935 [PubMed: 19329995]

19. Barker N, et al. Lgr5(+ve) stem cells drive self-renewal in the stomach and build long-lived gastric units in vitro. Cell stem cell. 2010; 6:25–36. DOI: 10.1016/j.stem.2009.11.013 [PubMed: 20085740]

20. Huch M, et al. In vitro expansion of single Lgr5+ liver stem cells induced by Wnt-driven regeneration. Nature. 2013; 494:247–250. DOI: 10.1038/nature11826 [PubMed: 23354049]

21. Dekkers JF, et al. A functional CFTR assay using primary cystic fibrosis intestinal organoids. Nature medicine. 2013; 19:939–945. DOI: 10.1038/nm.3201

22. Wei K, Kuhnert F, Kuo CJ. Recombinant adenovirus as a methodology for exploration of physiologic functions of growth factor pathways. Journal of molecular medicine. 2008; 86:161–169. DOI: 10.1007/s00109-007-0261-7 [PubMed: 17891365]

23. Wang B, Zhao L, Fish M, Logan CY, Nusse R. Self-renewing diploid Axin2(+) cells fuel homeostatic renewal of the liver. Nature. 2015; 524:180–185. DOI: 10.1038/nature14863 [PubMed: 26245375]

24. Benhamouche S, et al. Apc tumor suppressor gene is the “zonation-keeper” of mouse liver. Developmental cell. 2006; 10:759–770. DOI: 10.1016/j.devcel.2006.03.015 [PubMed: 16740478]

25. Planas-Paz L, et al. The RSPO-LGR4/5-ZNRF3/RNF43 module controls liver zonation and size. Nat Cell Biol. 2016; 18:467–479. ncb3337 [pii]. DOI: 10.1038/ncb3337 [PubMed: 27088858]

26. Lemmon MA, Schlessinger J. Transmembrane signaling by receptor oligomerization. Methods in molecular biology. 1998; 84:49–71. DOI: 10.1385/0-89603-488-7:49 [PubMed: 9666441]

27. Spangler JB, Moraga I, Mendoza JL, Garcia KC. Insights into cytokine-receptor interactions from cytokine engineering. Annual review of immunology. 2015; 33:139–167. DOI: 10.1146/annurev-immunol-032713-120211

28. Xu Q, et al. Vascular development in the retina and inner ear: control by Norrin and Frizzled-4, a high-affinity ligand-receptor pair. Cell. 2004; 116:883–895. [PubMed: 15035989]

29. Ke J, et al. Structure and function of Norrin in assembly and activation of a Frizzled 4-Lrp5/6 complex. Genes & development. 2013; 27:2305–2319. DOI: 10.1101/gad.228544.113 [PubMed: 24186977]
30. Chang TH, et al. Structure and functional properties of Norrin mimic Wnt for signalling with Frizzled4, Lrp5/6, and proteoglycan. eLife. 2015:4.
31. Veeman MT, Slusarski DC, Kaykas A, Louie SH, Moon RT. Zebrafish prickle, a modulator of noncanonical Wnt/Fz signaling, regulates gastrulation movements. Current biology : CB. 2003; 13:680–685. [PubMed: 12699626]
32. Biechele TL, Moon RT. Assaying beta-catenin/TCF transcription with beta-catenin/TCF transcription-based reporter constructs. Methods in molecular biology. 2008; 468:99–110. DOI: 10.1007/978-1-59745-249-6_8 [PubMed: 19099249]
33. Cooper S, et al. Predicting protein structures with a multiplayer online game. Nature. 2010; 466:756–760. DOI: 10.1038/nature09304 [PubMed: 20686574]
34. Azoitei ML, et al. Computation-guided backbone grafting of a discontinuous motif onto a protein scaffold. Science. 2011; 334:373–376. DOI: 10.1126/science.1209368 [PubMed: 22021856]
35. Fleishman SJ, et al. RosettaScripts: a scripting language interface to the Rosetta macromolecular modeling suite. PloS one. 2011; 6:e20161. [PubMed: 21731610]
36. Whitehead TA, et al. Optimization of affinity, specificity and function of designed influenza inhibitors using deep sequencing. Nature biotechnology. 2012; 30:543–548. DOI: 10.1038/nbt.2214
37. Kunkel TA. Rapid and efficient site-specific mutagenesis without phenotypic selection. Proceedings of the National Academy of Sciences of the United States of America. 1985; 82:488–492. [PubMed: 3881765]
38. Chao G, Cochran JR, Wittrup KD. Fine epitope mapping of anti-epidermal growth factor receptor antibodies through random mutagenesis and yeast surface display. Journal of molecular biology. 2004; 342:539–550. DOI: 10.1016/j.jmb.2004.07.053 [PubMed: 15327953]
39. Kabsch W. Xds. Acta crystallographica. Section D, Biological crystallography. 2010; 66:125–132. DOI: 10.1107/S0907444909047337 [PubMed: 20124692]
40. McCoy AJ, et al. Phaser crystallographic software. Journal of applied crystallography. 2007; 40:658–674. DOI: 10.1107/S0021889807021206 [PubMed: 19461840]
41. Emsley P, Cowtan K. Coot: model-building tools for molecular graphics. Acta crystallographica. Section D, Biological crystallography. 2004; 60:2126–2132. DOI: 10.1107/S0907444904019158 [PubMed: 15572765]
42. Adams PD, et al. PHENIX: a comprehensive Python-based system for macromolecular structure solution. Acta crystallographica. Section D, Biological crystallography. 2010; 66:213–221. DOI: 10.1107/S0907444909052925 [PubMed: 20124702]
43. Chen VB, et al. MolProbity: all-atom structure validation for macromolecular crystallography. Acta crystallographica. Section D, Biological crystallography. 2010; 66:12–21. DOI: 10.1107/S0907444909042073 [PubMed: 20057044]
44. Chao G, et al. Isolating and engineering human antibodies using yeast surface display. Nature protocols. 2006; 1:755–768. DOI: 10.1038/nprot.2006.94 [PubMed: 17406305]
45. Boder ET, Wittrup KD. Yeast surface display for directed evolution of protein expression, affinity, and stability. Methods in enzymology. 2000; 328:430–444. [PubMed: 11075358]
46. Los GV, et al. HaloTag: a novel protein labeling technology for cell imaging and protein analysis. ACS chemical biology. 2008; 3:373–382. DOI: 10.1021/cb800025k [PubMed: 18533659]
47. Gautier A, et al. An engineered protein tag for multiprotein labeling in living cells. Chemistry & biology. 2008; 15:128–136. DOI: 10.1016/j.chembiol.2008.01.007 [PubMed: 18291317]
48. Muster B, et al. Respiratory chain complexes in dynamic mitochondria display a patchy distribution in life cells. PloS one. 2010; 5:e11910. [PubMed: 20689601]
49. Lochte S, Waichman S, Beutel O, You C, Piehler J. Live cell micropatterning reveals the dynamics of signaling complexes at the plasma membrane. The Journal of cell biology. 2014; 207:407–418. DOI: 10.1083/jcb.201406032 [PubMed: 25385185]

50. Wilmes S, et al. Receptor dimerization dynamics as a regulatory valve for plasticity of type I interferon signaling. The Journal of Cell Biology. 2015; 209:579–593. DOI: 10.1083/jcb.201412049 [PubMed: 26008745]
51. Chen B, et al. Small molecule-mediated disruption of Wnt-dependent signaling in tissue regeneration and cancer. Nature chemical biology. 2009; 5:100–107. DOI: 10.1038/nchembio.137 [PubMed: 19125156]
52. VandeVondele S, Voros J, Hubbell JA. RGD-grafted poly-L-lysine-graft-(polyethylene glycol) copolymers block non-specific protein adsorption while promoting cell adhesion. Biotechnology and bioengineering. 2003; 82:784–790. DOI: 10.1002/bit.10625 [PubMed: 12701144]
53. Vogelsang J, et al. A reducing and oxidizing system minimizes photobleaching and blinking of fluorescent dyes. Angew Chem-Ger Edit. 2008; 47:5465–5469. DOI: 10.1002/anie.200801518
54. Thompson RE, Larson DR, Webb WW. Precise nanometer localization analysis for individual fluorescent probes. Biophysical journal. 2002; 82:2775–2783. DOI: 10.1016/S0006-3495(02)75618-X [PubMed: 11964263]
55. Gould TJ, Verkhusha VV, Hess ST. Imaging biological structures with fluorescence photoactivation localization microscopy. Nature protocols. 2009; 4:291–308. DOI: 10.1038/nprot.2008.246 [PubMed: 19214181]
56. Serge A, Bertaux N, Rigneault H, Marguet D. Dynamic multiple-target tracing to probe spatiotemporal cartography of cell membranes. Nature methods. 2008; 5:687–694. DOI: 10.1038/nmeth.1233 [PubMed: 18604216]
57. Schütz GJ, Schindler H, Schmidt T. Single-molecule microscopy on model membranes reveals anomalous diffusion. Biophysical journal. 1997; 73:1073–1080. doi:http://dx.doi.org/10.1016/S0006-3495(97)78139-6. [PubMed: 9251823]
58. You C, et al. Electrostatically Controlled Quantum Dot Monofunctionalization for Interrogating the Dynamics of Protein Complexes in Living Cells. ACS Chemical Biology. 2013; 8:320–326. DOI: 10.1021/cb300543t [PubMed: 23186299]
59. Wedeking T, et al. Single Cell GFP-Trap Reveals Stoichiometry and Dynamics of Cytosolic Protein Complexes. Nano Letters. 2015; 15:3610–3615. DOI: 10.1021/acs.nanolett.5b01153 [PubMed: 25901412]
60. Shah SM, Kang YJ, Christensen BL, Feng AS, Kollmar R. Expression of Wnt receptors in adult spiral ganglion neurons: frizzled 9 localization at growth cones of regenerating neurites. Neuroscience. 2009; 164:478–487. DOI: 10.1016/j.neuroscience.2009.08.049 [PubMed: 19716861]
61. Zhong ZA, Ethen NJ, Williams BO. Use of Primary Calvarial Osteoblasts to Evaluate the Function of Wnt Signaling in Osteogenesis. Methods in molecular biology. 2016; 1481:119–125. DOI: 10.1007/978-1-4939-6393-5_13 [PubMed: 27590158]
62. van de Wetering M, et al. Prospective derivation of a living organoid biobank of colorectal cancer patients. Cell. 2015; 161:933–945. DOI: 10.1016/j.cell.2015.03.053 [PubMed: 25957691]
63. Sato T, et al. Long-term expansion of epithelial organoids from human colon, adenoma, adenocarcinoma, and Barrett's epithelium. Gastroenterology. 2011; 141:1762–1772. DOI: 10.1053/j.gastro.2011.07.050 [PubMed: 21889923]
64. Bartfeld S, et al. In vitro expansion of human gastric epithelial stem cells and their responses to bacterial infection. Gastroenterology. 2015; 148:126–136e126. DOI: 10.1053/j.gastro.2014.09.042 [PubMed: 25307862]
65. Stange DE, et al. Differentiated Troy+ chief cells act as reserve stem cells to generate all lineages of the stomach epithelium. Cell. 2013; 155:357–368. DOI: 10.1016/j.cell.2013.09.008 [PubMed: 24120136]
66. Boj SF, et al. Organoid models of human and mouse ductal pancreatic cancer. Cell. 2015; 160:324–338. DOI: 10.1016/j.cell.2014.12.021 [PubMed: 25557080]
67. Huch M, et al. Unlimited in vitro expansion of adult bi-potent pancreas progenitors through the Lgr5/R-spondin axis. The EMBO journal. 2013; 32:2708–2721. DOI: 10.1038/emboj.2013.204 [PubMed: 24045232]
68. Huch M, et al. Long-term culture of genome-stable bipotent stem cells from adult human liver. Cell. 2015; 160:299–312. DOI: 10.1016/j.cell.2014.11.050 [PubMed: 25533785]

69. Wei K, et al. A liver Hif-2alpha-Irs2 pathway sensitizes hepatic insulin signaling and is modulated by Vegf inhibition. Nat Med. 2013; 19:1331–1337. nm.3295 [pii]. DOI: 10.1038/nm.3295 [PubMed: 24037094]

70. Rocha AS, et al. The Angiocrine Factor Rspondin3 Is a Key Determinant of Liver Zonation. Cell reports. 2015; 13:1757–1764. DOI: 10.1016/j.celrep.2015.10.049 [PubMed: 26655896]

71. Wagers AJ, Sherwood RI, Christensen JL, Weissman IL. Little evidence for developmental plasticity of adult hematopoietic stem cells. Science. 2002; 297:2256–2259. DOI: 10.1126/science.1074807 [PubMed: 12215650]

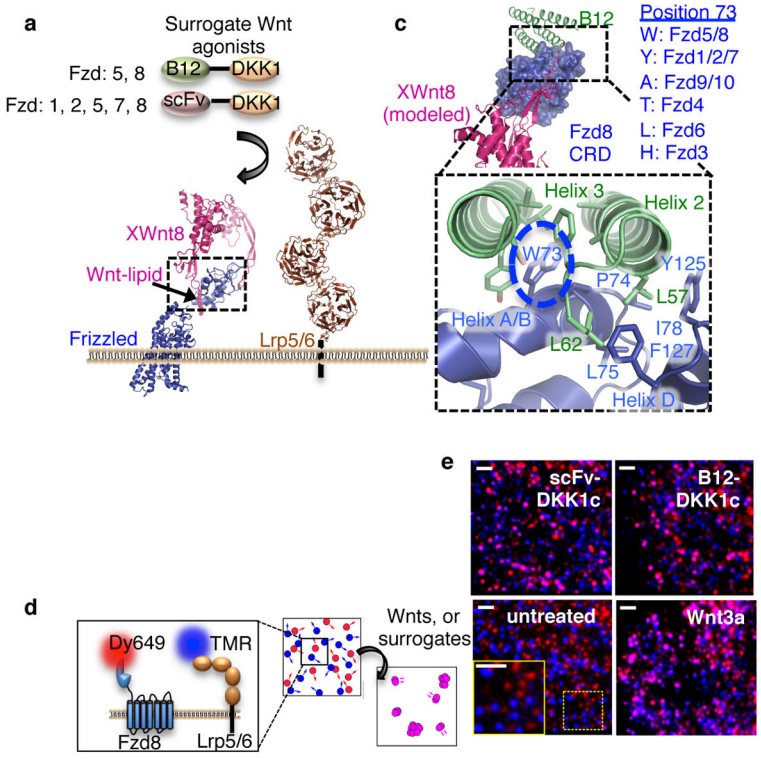

Figure 1. Engineering of Frizzled-specific and cross-reactive Lrp6/Fzd heterodimerizers

a, Concept of Wnt surrogate induced heterodimerization of Fzd and Lrp5/6. **b,** Binding affinities and specificities of B12 and scFv, determined by surface plasmon resonance (1), and yeast surface binding titration (2). Nb: no binding. **c**, Crystal structure of B12 (green) bound to Fzd8-CRD (blue), with modeled binding of XWnt8 and Wnt lipid (purple). Zoomed-in view of the B12-Fzd8-CRD binding interface with side chains mediating critical contacts shown in sticks. Residues that substitute for Trp73 in different Fzds are listed. Crystallographic data and refinement statistics are summarized in Supplementary Info Table 1. **d–e**, Schematic representation and typical single molecule fluorescence images for Fzd8 (red) and Lrp6 (blue) co-locomotion (magenta) mediated by scFv-DKK1c, B12-DKK1c, and Wnt3a in the plasma membrane of HeLa cells. Scale bars: 2 μm.

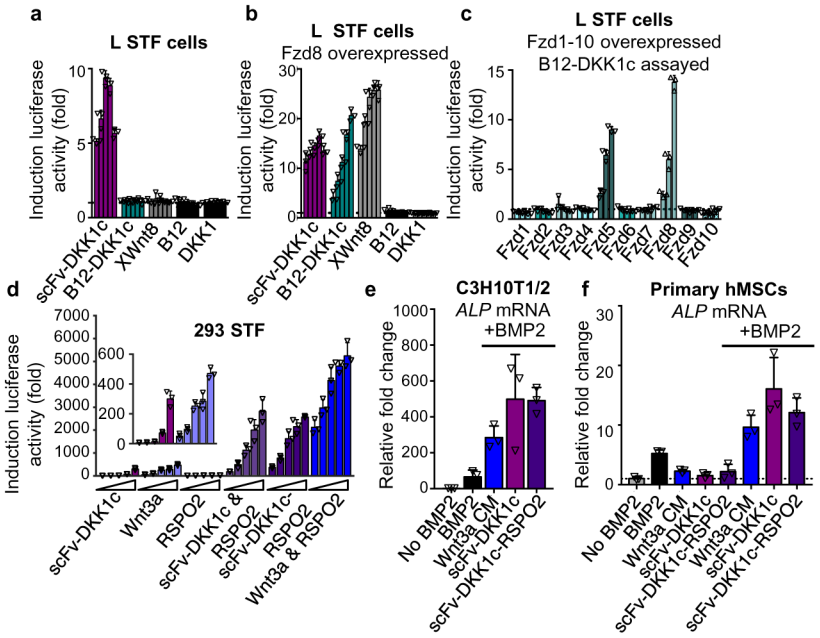

Figure 2. Fzd-specific activation of canonical Wnt signaling by Wnt surrogates

a–b, Activation of the β-catenin dependent STF reporter by Wnt surrogates, XWnt8 or negative control proteins (3–50nM) in L-cells (endogenously expressing Fzd7) without (a) and with (b) overexpression of Fzd8. **c,** Activation of the STF reporter by B12-DKK1c (5, 25, 100 nM) in L-cells overexpressing the ten mouse Fzds. **d**, RSPO2 (5–75nM) potentiates the activity of scFv-DKK1 (5–75nM) and Wnt3a CM (25–45%) demonstrated by the enhanced expression of the STF reporter in HEK293 cells. The scFv-DKK1c-RSPO2 fusion replicates the enhanced activity of the individual proteins. **e**, Up-regulation of *ALP* mRNA, an early osteogenic marker in C3H10T1/2 cells treated for 4 days with Wnt3a CM, 50 nM scFv-DKK1c and 50 nM scFv-DKK1c-RSPO2 in the presence of 200 ng/ml BMP2 in osteogenic media. **f**, Up-regulation of *ALP* mRNA in human primary MSC treated for 3 days with Wnt3a, 50 nM scFv-DKK1c and 50 nM scFv-DKK1c-RSPO2 in the presence and absence of 200 ng/ml BMP2. Error bars represent S.D. of n=3 technical replicates from one of 3 (a,b,c, e, f) and 5 (d) representative experiments.

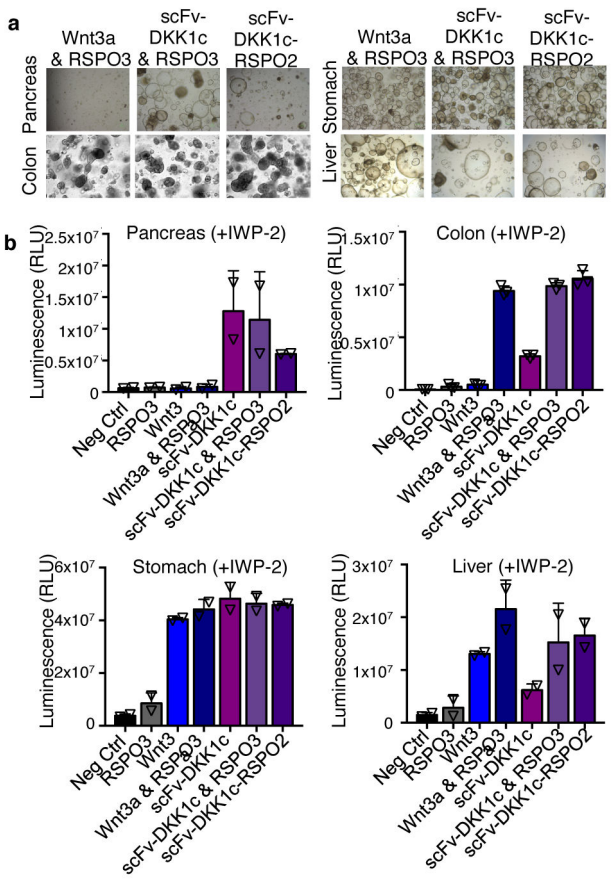

Figure 3. Activity of Wnt surrogates on human organoid cultures *in vitro*

a, Representative bright-field images of organoids of human pancreas, colon, stomach (corpus), and liver expanded for 12 days in basal media containing 3 μM IWP-2 and tissue specific growth factors (Supplementary Info Table 2), and supplemented with 50% Wnt3a-CM + 2% RSPO3-CM, 200 nM scFv-DKK1c + 2% RSPO3-CM and 200 nM scFv-DKK1c-RSPO2. **b**, Quantification of cell proliferation and organoid expansion (live cells based on the presence of intracellular ATP in metabolically active cells) by luminescence. Bars and error bars represent mean and S.D. from n=2 (pancreas, liver and stomach) and n=3 (liver) technical replicates from one of 3 (colon), 2 (liver and pancreas) and 1 (stomach) representative experiments.

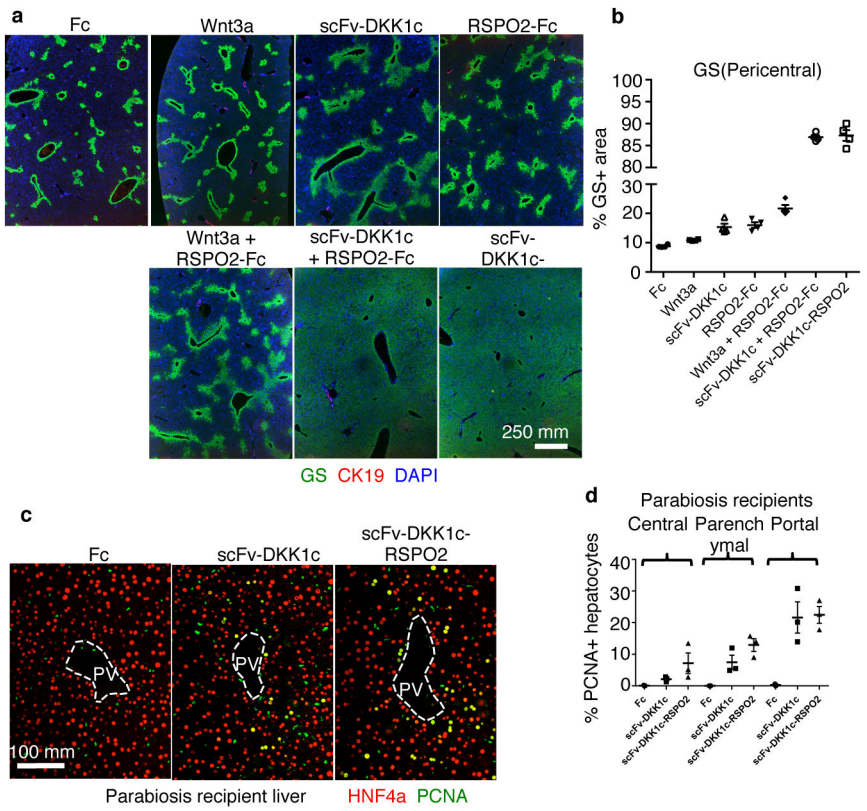

Figure 4. Engineered Wnt surrogate is bioactive and up-regulates Wnt signaling *in vivo*

a, Representative images of GS (pericentral marker) and CK19 (bile duct/portal marker) immunofluorescence staining of livers from mice that received adenoviruses expressing mouse IgG Fc (Fc), mouse Wnt3a, scFv-DKK1c, human RSPO2-Fc, Wnt3a + RSPO2-Fc, scFv-DKK1c + RSPO2-Fc or scFv-DKK1c-RSPO2, 7 days post adenovirus injection (n=4 mice/group). **b,** Quantification of the GS immunofluorescence staining area shown in (a) relative to liver tissue area, with vessel lumen area subtracted (*n*=4 mice/group). **c–d,** Effects of scFv-DKK1c and scFv-DKK1c-RSPO2 on hepatocyte proliferation determined in surgically paired by parabiosis. The donor mice received adenoviruses i.v. two days prior parabiosis surgery with recipient mice to establish cross-circulation to allow diffusion of the transgenes in both mice. Immunofluorescent staining (c) and quantification of proliferating hepatocytes (d) in recipients mice with PCNA and HNF4α 7 days after parabiosis surgery. PV, portal vein. *n*=3 mice/group. Experiments demonstrating the regulation of liver zonation were performed at least 2x for each condition (n=4 mice/group), parabiosis experiment was done 1 time in the lab (n=3 mice/group). Error bars represent S.E. from biological replicates.